Pelvic Responses and Injuries to Male Post-Mortem Human Subjects (PMHS) in Rear-facing Seat Configurations in High-speed Frontal Impacts

Yun-Seok Kang, Vikram Pradhan, Jason Stammen, Gretchen H. Baker, Angelo Marcallini, Amanda M. Agnew, Kevin Moorhouse, John H. Bolte IV

Abstract This study explored biomechanical responses and injuries of post-mortem human subject (PMHS) pelves with varying boundary conditions in high-speed rear-facing frontal impacts (HSRFFI). Thirteen male PMHS tests (10 PMHS from previous studies and 3 additional PMHS included) were conducted at ΔV of 56km/h and input acceleration of 37g using two recline angles (25deg and 45deg) and two reinforced seats: 1) a 2018 Honda Odyssey with All Belts To Seat (ABTS) restraint (N=3 for ABTS25, N=3 for ABTS45) and 2) a 2018 Honda Accord with Fixed D-ring (FDR) seat belt (N=4 for FDR25, N=3 for FDR45). The PMHS tested in ABTS25 did not experience any fractures, while two PMHS tested in ABTS45 sustained sacroiliac (SI) joint damage and fractures throughout the pelvis. The PMHS tested in both FDR conditions sustained SI damage and posterior ilium fractures due to seat back interaction. For FDR25, the PMHS exhibited larger forward y-angular velocities than ABTS25. Three PMHS tested in the FDR conditions sustained pubic ramus fractures due to open-book deformation from large z-angular velocities (a potential injury predictor). Two loading mechanisms were identified: 1) direct pelvis interaction with the seat back and 2) lower extremity inertial loading applied to the pelvis through the acetabulum. Seat back structures influenced y-angular velocities and x-linear acceleration, which might also affect pelvis injuries from HSRFFI.

Keywords Injury mechanism, pelvis fracture, pelvis open-book, rear-facing, seat back structure.

I. INTRODUCTION

Motor vehicle automation, ranging from Level 0 (no driving automation) to Level 5 (full driving automation), has been classified [1] and developed by automakers and researchers. Motor vehicle automation has received considerable attention, and tremendous efforts have been made by automakers toward implementation of automated features. Despite this, full driving automation has not yet been achieved and is still under research and development. Regardless of the progress of full driving automation, occupant safety should be prioritised for vehicles with an automated driving system (ADS). Given occupants may not be required to drive vehicles equipped with ADS, especially Level 4 and 5 vehicles, concept designs of alternative seating configurations have been proposed in the literature [2-3]. However, it is unknown if the non-conventional seating configurations in vehicles with ADS are capable of providing equivalent levels of occupant safety as the forward facing configurations in current vehicles.

Consumer surveys have suggested a potential desire for numerous unconventional seating configurations if vehicles with ADS are operated on the roads [2-4]. Consumers prefer rear-facing seat configurations, i.e., living room or campfire seating condition, when travelling long distances with children and family members [2-3]. However, information regarding occupant injury risk in high-speed rear-facing frontal impacts (HSRFFIs) is very sparse in the literature, so evaluation of biomechanical responses and injuries in HSRFFIs are required to enhance the ability of safety tools, such as anthropomorphic test devices (ATDs) and human body models (HBMs), to represent realistic occupant responses and injury risk in HSRFFIs.

Recently, a series of post-mortem human subject (PMHS) sled tests were conducted in HSRFFIs at ΔV of 56 km/h to investigate biomechanical responses and injuries (hereafter referred to as “Kang studies”) [5-7]. The previous Kang studies [5-7] examined the effect of two seat back recline angles (25deg and 45deg), two reinforced original equipment manufacturer (OEM) seats, and two seat belt conditions, specifically a 2018 Honda Odyssey

Y-S. Kang is an Associate Professor (tel: +1 614 366 7584, e-mail: yunseok.kang@osumc.edu), V. Pradhan, G. Baker, A. Marcallini, A. Agnew, and J. Bolte are student, staff, and faculty in the Injury Biomechanics Research Center at the Ohio State University in Columbus, OH, USA. J. Stammen and K. Moorhouse are at the National Highway Traffic Safety Administration (NHTSA), in East Liberty, OH, USA.

with All-Belts-To-Seat (ABTS) restraint and a 2018 Honda Accord with Fixed D-ring (FDR) seat belt. The ABTS condition was used to minimize the risk of the PMHS ejection from the seat and could simulate the most likely belt system for alternative seating configuration [5]. Since different seat properties and restraint systems could possibly affect PMHS responses and injury outcomes, the FDR condition was also used to investigate PMHS responses and injuries in HSRFFIs [6]. Biomechanical responses for the head, thorax (chest deflection and kinematics at T1, T4, T8, and T12), pelvis, femora, and tibiae were reported in the Kang studies [5-7]. Large ramping-up motions of the PMHS were observed in both recline conditions, in particular at the 45deg recline angle. PMHS injuries reported in the studies [5-7] included minor cervical spine injuries due to loads from the head restraint, scapula fractures due to the retractor structure in the seat back frame, clavicle and ulna fractures due to flailing of the upper extremity, and fibula and tibia fractures due to interaction with the front seat pan. Major injuries sustained by the PMHS were rib and pelvis fractures.

Rib fractures and injury mechanisms have been discussed in a recent study [7]. PMHS sustained a greater number of rib fractures (NRF) in the reclined (45-degree) seat conditions (ABTS45 and FDR45) than in the upright (25-degree) seat conditions (ABTS25 and FDR25). Anterior-to-posterior (A-P) chest deflections of the PMHS and strain magnitudes measured along the ribs did not correlate with the NRF in HSRFFIs. A potential injury mechanism, which was identified as a combination of A-P with inferior-to-superior (I-S) chest deflection, was discovered in the previous study [7]. Since all PMHS except one sustained rib fractures, rib fracture mechanisms have been explored primarily in the previous study.

Nine PMHS (N=2 for ABTS45, N=3 for FDR45, N=0 for ABTS25, and N=4 for FDR25) out of 13 PMHS in the Kang studies [5-7] also sustained pelvic injuries (6 PMHS out of 9 sustained AIS3+), likely due to the interaction of the seat back. These types of injuries are severe and require a long recovery time if sustained in life. However, pelvic injury types and injury locations associated with pelvis kinematics in HSRFFI have not yet been discussed. Literature for pelvic responses and injuries in HSRFFIs or any rear impacts is sparse. Prior to concerns about pelvic injuries in HSRFFIs, only a few studies had explored pelvic responses of PMHS and human volunteers in low-to-moderate speed rear impacts [8-10].

Davidsson et al. (1998) [8] investigated human volunteer kinematics (N=13, 12 males and one female) and seat design influences on biomechanical responses in low-speed rear impacts (ΔV of 5kph and 7kph). One production seat and two versions of experimental seats that mimicked two different seat back stiffnesses (stiff vs. more extension of the torso) were used to explore the influence of different seat designs on volunteer responses. Peak pelvic linear accelerations (< 60m/s^2 in x-direction) and H-point displacement (< 80mm in x-direction and 25mm ramping in z-direction) were reported in the study. However, the main goal of the study was to provide accurate biomechanical corridors for ATD head and neck evaluation, so pelvic responses were not discussed in detail. Moreover, no angular kinematics data were measured in the study.

Philippens et al. (2000) [9] performed rear impact sled tests using five PMHS (four female and one male) at ΔV of 16 and 25kph in order to generate biomechanical responses of 5th and 95th percentile PMHS. Two female PMHS were seated in a rigid seat without seat foam (called upholstery), while the remaining PMHS were tested with seat foam. Photo targets were attached to the pelvis to quantify pelvis displacement and rotation. In tests with the seat foam, peak pelvis x- and z-displacements were approximately 97mm (x) and 44mm (z) for the male and 24mm (x) and 20mm (z) for the female. The pelvis forward rotations were also reported (19deg for males, 8deg for females), but head-to-T1 and T1-to-pelvis relative kinematics, along with neck loads, were the primary focus in the study. Even though the study provided pelvis linear and angular displacements, pelvic accelerations were not reported.

White et al. (2009) [10] conducted a series of rear impact PMHS sled tests using a mini-sled at ΔV of 8kph without a head restraint and 16kph with a head restraint. A rigid seat back (20-degree) and seat pan were used in the study. A 3-2-2-2 accelerometer package was installed at the right iliac crest to quantify six degrees of freedom (6DOF) pelvis kinematics in rear-ended impact conditions. Peak linear pelvic acceleration in the x-direction was approximately 94m/s^2 in the 16kph test. Angular kinematics about the y-axis, such as angular acceleration (-677 to 519rad/s^2), angular velocity (-11.3 to 11.5rad/s), and rotation (-11.6 to 3.5deg) were also reported in the study. Head, cervical, and T1 kinematics relative to the pelvis kinematics were mainly discussed since understanding cervical spine injuries in low-to-moderate speed rear impacts was the main goal of the study. Although the pelvis linear and angular kinematics were reported, information regarding how the pelvis motions affected injury outcomes was not included. Given these studies mainly focused on head, neck, and spine

kinematics for low-to-moderate speed rear impacts, pelvic kinematics, injuries, and injury mechanisms have not been explored. Therefore, this study aimed to explore pelvic injury types, locations, mechanisms, and relevant biomechanical responses of male PMHS with varying boundary conditions in HSRFFIs.

II. METHODS

PMHS Characteristics

Thirteen male PMHS used in this study were previously tested in HSRFFI scenarios (37g and ΔV of 56km/h), as described in the Kang studies [5-7]. Pelvis responses (e.g., global and local kinematics from one iliac wing) from ten PMHS have been discussed in [5-6], while those from three additional PMHS (PMHS10, PMHS21, PMHS22 in Table I) have not been published. PMHS characteristics are summarised in Table I. The average PMHS age was 61 ± 5 years (ranging from 53 to 71 years). For PMHS body size, average PMHS height (176 ± 4.8cm) and weight (80 ± 12.7kg) were comparable to a 50th percentile male (175cm and 78.2kg from [11]). PMHS seated heights (94.3 ± 2.3cm) were slightly taller than the 50th percentile male (90.7cm). Areal bone mineral density (aBMD) measured using a Dual-Energy X-ray Absorptiometry (DEXA) ranged from -1.4 to 1.9 in the lumbar region (L2–L4). Anthropometrics relevant to the pelvis of the PMHS are also provided in Table A1 (see Appendix A).

TABLE I
PMHS CHARACTERISTICS AND TEST MATRIX

Test condition	PMHS#	Sex	Age (yr)	Height (cm)	Weight (kg)	Seated height (cm)	aBMD L2-L4 T-score[#]
ABTS45	PMHS01[*]	M	57	167.0	62.6	90.0	1.9
	PMHS04[*]	M	59	178.0	96.2	96.5	-0.1
	PMHS05[*]	M	62	176.0	77.1	95.7	-1.0
FDR45	PMHS09[**]	M	71	187.5	89.4	96.5	-0.4
	PMHS13[**]	M	53	176.3	76.2	95.7	1.9
	PMHS22[***]	M	61	176.6	71.7	94.1	-1.0
ABTS25	PMHS02[*]	M	64	171.0	62.6	92.4	0.7
	PMHS03[*]	M	54	174.0	93.9	97.0	1.2
	PMHS06[*]	M	61	176.5	72.6	94.0	-1.4
FDR25	PMHS10[***]	M	62	177.8	100.7	94.5	-0.1
	PMHS11[**]	M	65	181.0	92.1	96.5	1.3
	PMHS12[**]	M	58	177.8	71.7	94.2	1.9
	PMHS21[***]	M	62	172.7	68.5	89.7	-0.1
Mean (SD)	N/A	N/A	61 (5)	176.3 (4.9)	79.6 (13.1)	94.4 (2.4)	0.4 (1.2)
50th Male[****]	N/A	N/A	45	175.0	78.2	90.7	N/A

* [5]; ** [6]; ***[7]; **** [11]
# aBMD deselection criterion was L2-L4 T-score less than -2.5

General Sled Setup

The PMHS were seated in two reinforced OEM seats (ABTS and FDR) with two different recline angles (25 and 45deg), as shown in Fig. 1. A summary of the test matrix, including the OEM seats and seat back recline angles for the PMHS, is shown in Table I. Internal frame structure and seat back foam thickness at various locations of the OEM seats are provided in Fig. 2. The ABTS seat back structure includes a retractor assembly installed on the left side of the seat back, which resulted in asymmetric shape of the seat back frame (Fig. 2a). The FDR seat back structure composes of serpentine springs (or seat back suspension) in the middle (Fig. 2b), which allows occupants pocket into the seat back during rear impact and rear-facing scenarios. Unlike the FDR seat back, the ABTS seat back has a top tether anchor bracket for the Lower Anchors and Tethers for Children (LATCH) system (Fig. 2a). Below the top tether anchor bracket, there is a crossbar that can interact with the superior aspect of the posterior pelvis. Seat foam thicknesses for the FDR seat are thinner than the ABTS seat shown in Fig. 2. Reinforced frames were installed behind the seat back and head restraint to ensure the durability and repeatability of the sled setup. The OEM seats, head restraints, and seat belts (no pretensioner) were replaced after each test. Further information for the experimental setup and PMHS positioning procedure was provided in [5-6].

(a) ABTS45 (PMHS05)

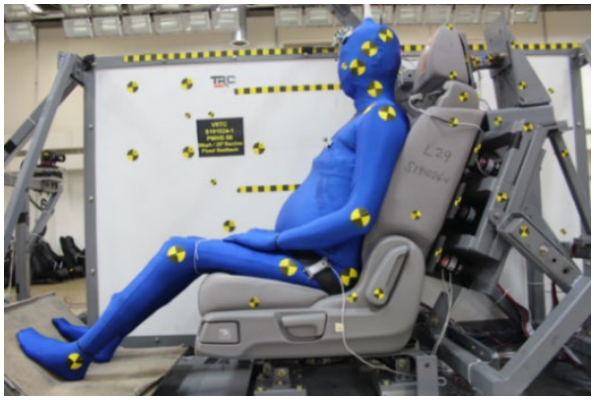

(b) ABTS25 (PMHS06)

(c) FDR45 (PMHS22)

(d) FDR25 (PMHS21)

Fig. 1. General experimental setup for each seat condition.

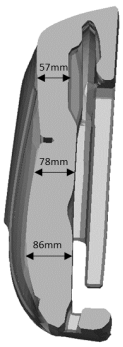

Seat back foam thickness

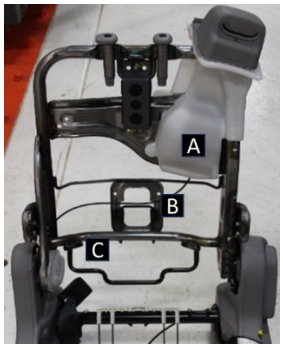

Seat back structure

(a) 2018 Honda Odyssey (ABTS)

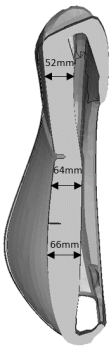

Seat back foam thickness

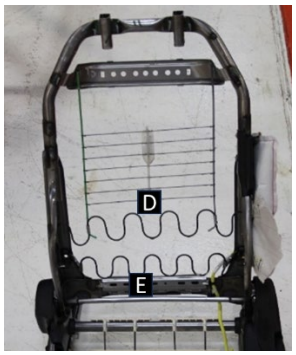

Seat back structure

(b) 2018 Honda Accord (FDR)

Fig. 2. Seat back foam thickness and structure.
A: retractor housing, B: top tether anchor bracket, C: crossbar, D: serpentine springs, and E: crossbar

Pelvic Instrumentation

A 6DOF motion block (6DX, DTS, Seal Beach, CA, USA) was installed on each iliac wing posterior to the anterior superior iliac spine (ASIS), shown in Fig. 3. The instrumentation mounts were secured to the iliac wing using bolts and nuts through two holes created with a 4.7mm (3/16 inch) drill bit. After installing instrumentation on each PMHS, a full-body computed tomography (CT) scan with 0.6mm slice thickness was performed, and a commercial 3D CT software (Mimics, Materialise, Plymouth, MI, USA) was used to digitise locations of the 6DX block and anatomic bony landmarks.

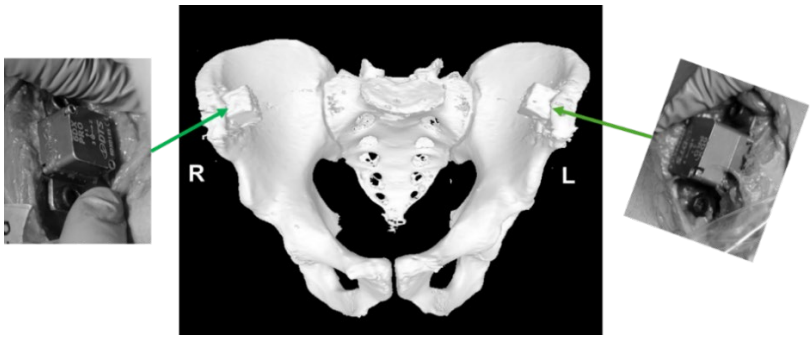

Fig. 3. Pelvic instrumentation. Images from instrumentation CT.

Data Acquisition and Analysis

PMHS data were recorded using a data acquisition system (SLICE PRO, DTS, Seal Beach, CA, USA) at 20,000 Hz sampling frequency, while sled data (sled acceleration, seat belt loads) were collected from a second data acquisition system (KT, Kayser-Threde, Munich, Germany) at 20,000 Hz sampling rate. Linear acceleration and angular velocity measured from the 6DOF motion block were filtered at CFC1000 and CFC180, respectively. Three onboard (front, oblique, and side) high-speed cameras (N3, Integrated Design Tools, Inc. Pasadena, CA, USA) were used to capture the PMHS overall motions at a 1,000 Hz sampling frequency.

The anatomical coordinate system of the pelvis used in the current and previous studies [5-6] is presented in Fig. 4. The local x-axis was defined using a unit vector defined from the centre of the posterior superior iliac spine

(PSIS) to the centre of the ASIS, while the local y-axis was a unit vector from the left ASIS to the right ASIS. The z-axis vector was computed using a cross-product between the unit vectors in x- and y-directions. One additional cross-product, e.g., z-vector cross x-vector, was performed to ensure orthogonality of the anatomical coordinate system of the pelvis. These three unit vectors in x-, y-, and z-directions were used to create a transformation matrix for the pelvic anatomical coordinate system. The 6DOF motion block coordinate system and its transformation matrix were defined by using the digitised motion block points and by following the same procedure used for the anatomical coordinate system. The 6DOF motion block data were transformed (translation) to the centre point between right and left PSIS, and then a rotational matrix that transformed (rotation) the motion block coordinate system to the anatomical coordinate system was applied to the data. Initial pelvic orientations were determined with X-ray images acquired after positioning the PMHS in the seats.

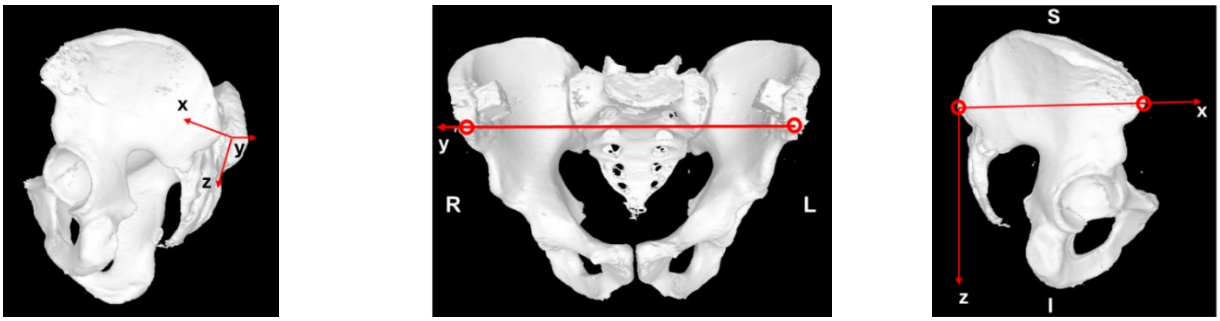

(a) pelvic coordinate system at origin of center of PSIS (b) y-axis vector (c) x- and z-axis vectors

Fig. 4. Pelvic coordinate system.

III. RESULTS

The pelvis injury types and locations of the PMHS tested in both ABTS and FDR conditions are shown in Fig. 5. Two out of three PMHS (PMHS04 and PMHS05) sustained pelvis fractures in ABTS45, while all three PMHS suffered pelvis fractures in FDR45. For ABTS45 (Fig. 5a), PMHS04 sustained fractures at the left PSIS and the right posterior ilium with sacroiliac (SI) joint damage, while PMHS05 had fractures at the left acetabulum, ischium, and iliopubic ramus. For FDR45 (Fig. 5b), PMHS09 had bilateral superior and inferior pubic ramus fractures as well as damage to the left and right SI joints. Both PMHS13 and PMHS22 sustained posterior ilium fractures. PMHS13 also had left SI joint damage. No pelvis fractures were sustained by the three PMHS tested in ABTS25. However, PMHS10 and PMHS12 tested in FDR25 sustained superior and inferior pubic ramus fractures and bilateral SI joint damage. PMHS11 had acetabular fractures with SI joint damage (not shown in the image), while PMHS21 sustained a fracture at the right PSIS.

Since peak values are typically used to evaluate injury criteria and risk, peak linear acceleration at the origin and peak angular velocity with respect to the pelvic coordinate system (Fig. 4) are presented in Tables II and III, respectively. Corresponding peak timing information is also provided in Tables AII and AIII. For the PMHS that sustained acetabular fractures (PMHS05 and PMHS11), peak magnitudes of the linear accelerations in all three x-, y-, and z-directions were greater than those measured from those PMHS without acetabular fractures (Table II). In addition, peak magnitudes of the angular velocities about x- and z-axes (off axes) in PMHS05 were greater than the PMHS tested in the same condition but without acetabular fractures (Table III). However, peak magnitudes of the angular velocities measured from PMHS11 were comparable to the other PMHS in the same condition (Table III). For the PMHS that sustained superior and inferior pubic rami fractures (PMHS09, PMHS10, and PMHS12), regardless of the seat type and recline angles, the magnitudes of the angular velocities about the z-axis that represent pelvic outward (open book) deformation [6] were much greater than for the other PMHS that did not sustain fractures. However, no consistent trends were observed in angular velocities about the x- and y-axes and linear accelerations in all directions when comparing PMHS with pubic rami fractures to ones without fractures. For the PMHS that sustained fractures of the posterior ilium, there were no obvious trends in linear accelerations or angular velocities (Tables II and III). Time histories of the linear accelerations and angular velocities are presented in Figs. A1 – A6. Sequential PMHS pelvic motions are illustrated in Fig. B1 to provide general pelvic motions during the events.

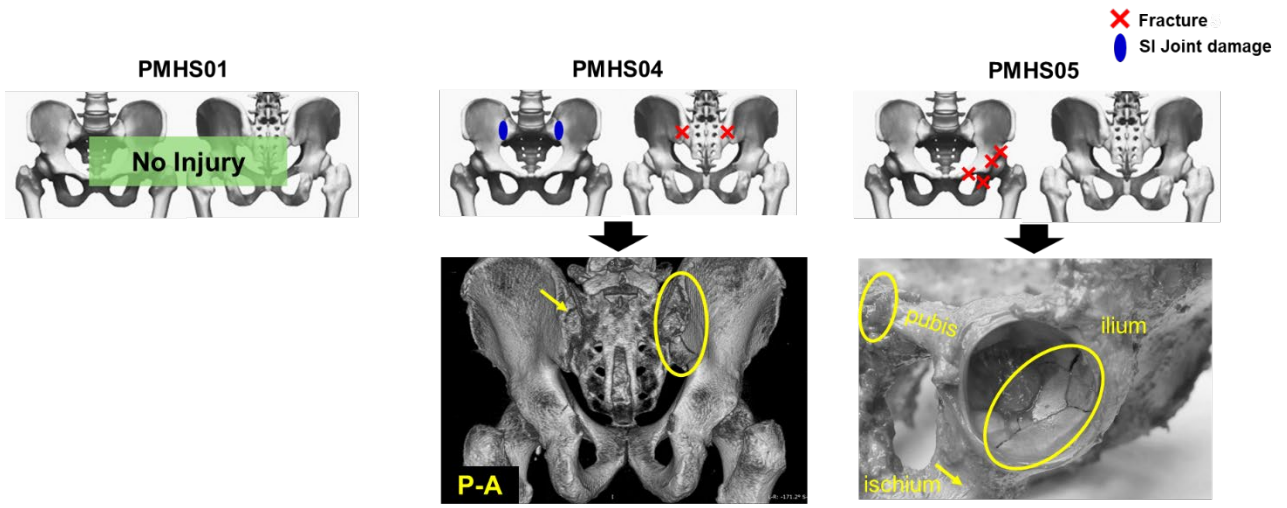

(a) ABTS45

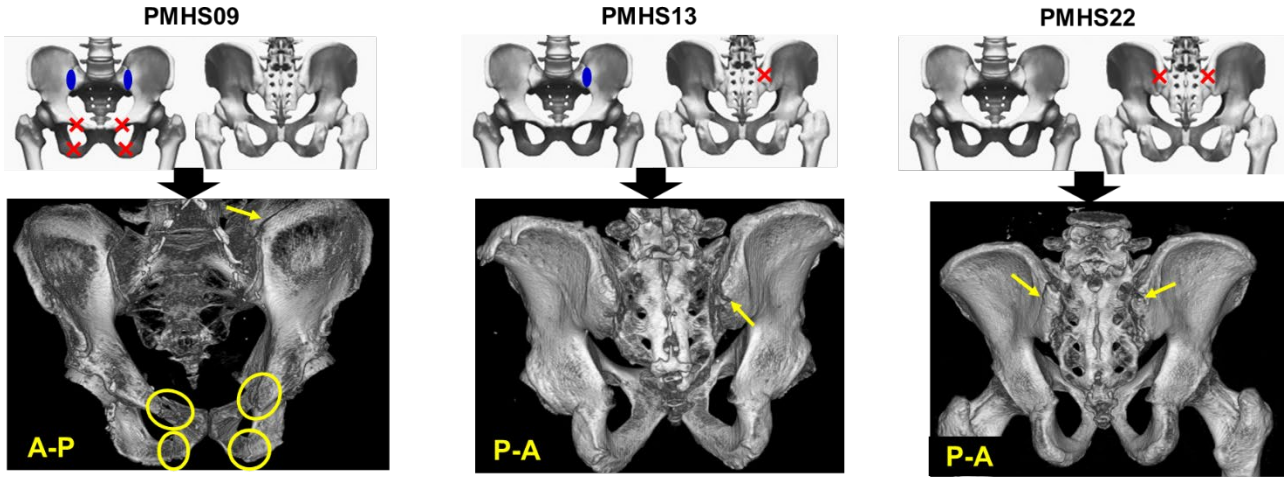

(b) FDR45

(c) ABTS25

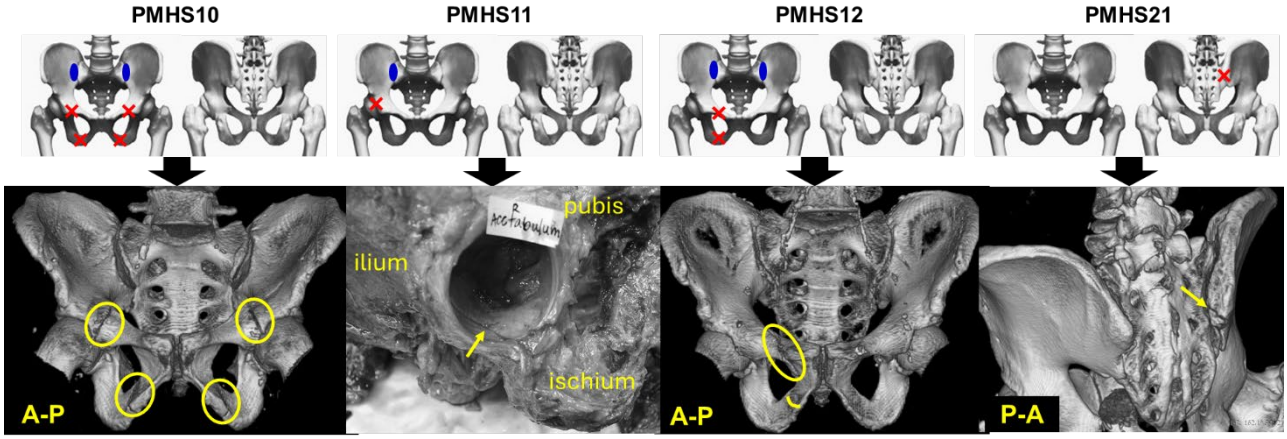

(d) FDR25

Fig. 5. Pelvis injuries and locations.

TABLE II
PEAK LINEAR ACCELERATION AT PELVIS ORIGIN

Test condition	PMHS#	x-direction		y-direction		z-direction	
		Left	Right	Left	Right	Left	Right
ABTS45	PMHS01	135.7	133.0	-75.0	-39.9	62.4	76.7
	PMHS04	121.4*	103.8*	47.2*	-69.0*	65.8*	59.5*
	PMHS05	297.1	127.7	-208.0	-96.0	295.7	56.4
FDR45	PMHS09	171.3*	141.1*	98.4*	-48.2*	-65.2*	48.3*
	PMHS13	131.2*	159.3	-37.4*	74.2	-43.8*	-50.4
	PMHS22	175.1	212.5	-165.3	216.3	-110.3	-73.2
ABTS25	PMHS02	166.5	160.7	-53.4	-33.8	-54.5	-58.9
	PMHS03	91.4	104.0	-28.1	-14.3	31.6	34.6
	PMHS06	126.5	120.3	15.0	-50.3	30.6	-15.7
FDR25	PMHS10	156.7*	169.4*	50.6*	-117.4*	88.5*	176.1*
	PMHS11	169.0	202.0*	-64.4	142.3*	69.8	219.9*
	PMHS12	166.4*	185.8*	-72.0*	-135.5*	-87.4*	-83.4*
	PMHS21	185.7	201.0	114.4	-88.9	-154.4	58.0

green: no pelvic fracture
blue: posterior ilium fracture
purple: acetabular fracture
red: pubic ramus fracture
*: sacroiliac joint damage

TABLE III
PEAK ANGULAR VELOCITY OF PELVIS

Test condition	PMHS#	x-direction		y-direction		z-direction	
		Left	Right	Left	Right	Left	Right
ABTS45	PMHS01	-247.6	339.9	1464.3	1454.8	-764.1	-493.9
	PMHS04	576.6*	446.0*	1430.0*	1401.9*	-238.4*	436.7*
	PMHS05	825.3	338.8	1321.1	1275.3	933.4	821.7
FDR45	PMHS09	-288.5*	429.7*	-1294.2*	-1152.8*	-1508.6*	1037.5*
	PMHS13	-183.2*	330.2	896.4*	942.4	-265.8*	330.4
	PMHS22	-551.1	371.5	987.2	951.2	-536.3	496.1
ABTS25	PMHS02	251.4	337.8	-1124.3	-1163.4	-282.7	298.9
	PMHS03	482.4	382.4	-629.9	-630.6	451.1	600.2
	PMHS06	361.2	511.2	-666.7	-704.1	250.9	308.0
FDR25	PMHS10	308.2*	753.9*	-2040.8*	-1896.2*	-1434.4*	1555.6*
	PMHS11	-383.9	269.5*	-1739.6	-1675.2*	-689.3	584.2*
	PMHS12	-388.2*	418.5*	-1521.5*	-1533.2*	-817.5*	1334.8*
	PMHS21	363.3	498.1	-1776.3	-1684.8	-1031.4	565.4

green: no pelvic fracture
blue: posterior ilium fracture
purple: acetabular fracture
red: pubic ramus fracture
*: sacroiliac joint damage

IV. DISCUSSION

Thirteen PMHS seated in two different seats with two reclined seat back angles were tested in a rear-facing sled environment at ΔV of 56kph. Nine out of thirteen PMHS sustained pelvic fractures. Pelvic fractures and locations, as well as relevant kinematics which provided insights into potential pelvic injury mechanisms, were investigated in this study.

Acetabular fractures of PMHS05 and PMHS11 were identified in peak linear acceleration results (Table II) and

time histories in the x-, y-, and z-directions (Figs. A1a, A1h, A2a, A2h, A3a, and A3h). PMHS05 sustained more extensive fractures than PMHS11 (Fig. 5), which might explain pronounced spikes and peaks in the x-, y-, and z-accelerations from PMHS05. For PMHS11, notable spikes and peaks were identified only in the y- and z-accelerations. Peak timings of the y- and z-accelerations ranged 46.80 - 47.20ms for PMHS05 and 46.15 - 47.15ms for PMHS11. When these notable spikes and peaks occurred, the PMHS translated into the seat back, and the pelvis interacted with the seat back (Fig. B1). In this phase, inertial loads induced from the lower extremities were continuously increased and applied to the pelvis through the acetabulum while the posterior aspect of the pelvis interacted with the seat back. The femur linear accelerations measured at the mid-shaft in the z-direction (femur axial loading direction according to SAEJ211 [12]) are shown in Fig. 6. The acetabular fracture signals (sudden deceleration at 43.85ms in Fig 6a and 46.30ms in Fig 6b) were also present in the femur accelerations, so iliac wing and femur 6DOF motion blocks successfully detected the fractures although spikes in the iliac wing accelerations occurred later than those in the femur accelerations.

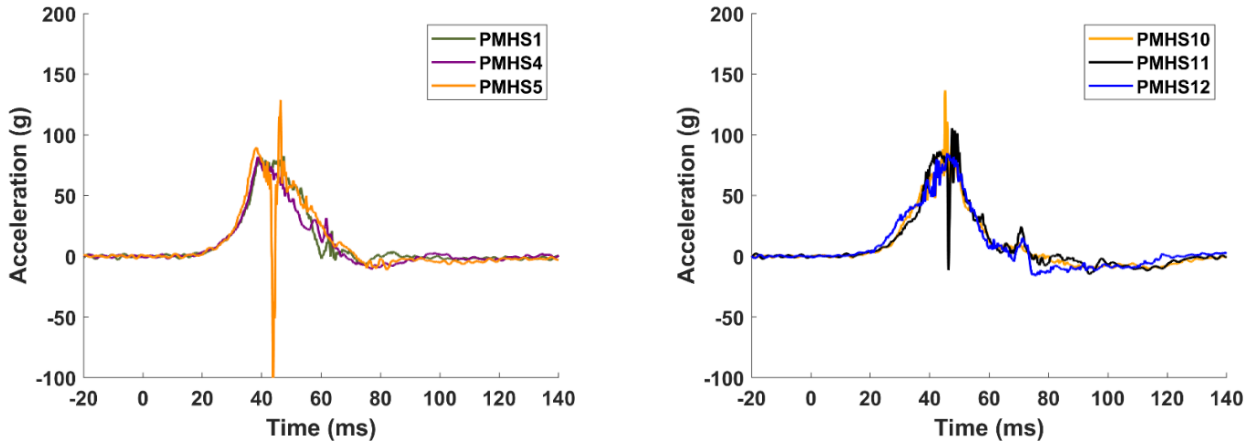

(a) ABTS45 left (b) FDR25 right

Fig. 6. Femur linear acceleration in the z-direction.

Acetabular fractures in PMHS have occurred in a well-controlled knee-thigh-hip (KTH) experiment [13], where PMHS pelves were mounted in a test fixture while impulse loading was applied through the knee. The average force ± one standard deviation at the time of acetabular fractures from the KTH impacts was 5.7 ± 1.3kN. In Fig. 6, peak femur z-accelerations for PMHS05 and PMHS11 were 89.3g (876.0m/s^2) and 86.5g (848.6m/s^2) prior to acetabular fractures (not including large spikes due to fracture). Mass properties of 10 male PMHS (175 ± 6cm and 79.4 ± 10.0kg) measured from a previous study [14] were incorporated with the femur acceleration data to estimate inertial loads induced from the lower limb. In the previous study, average thigh, leg, and foot masses were 6.8kg, 2.6kg, and 1.0kg (lower limb: 10.4kg), respectively. As a worst-case scenario, assuming the lower limb is a rigid body and experiences pure translation during rear-facing impacts, inertial loads from the lower limb would be approximately 8.8kN (10.4kg x 848.6m/s^2) – 9.1kN (10.4kg x 876.0m/s^2). When only considering thigh mass (6.8kg), the inertial force induced from the thigh would be approximately 5.8kN (6.8kg x 848.6m/s^2) – 6.0kN (6.8kg x 876.0m/s^2). Based on these estimations, inertial loads induced from the lower limb range from 5.8kN (thigh mass) to 9.1kN (lower limb mass), which are in the range of the acetabular fracture forces (3.9 – 8.9kN) reported in [13]. PMHS without acetabulum fractures (PMHS01, PMHS04, PMHS10, and PMHS12 shown in Fig. 6) also experienced 81.9g (5.5kN for thigh mass to 8.4kN for lower limb mass) to 88.2g (5.9kN for thigh mass to 9.0kN for lower limb mass). However, these PMHS sustained fractures at other locations (e.g., ilium and pubic rami), likely due to different energy transfer mechanisms from PMHS variation (e.g., geometric, material, and structural), except for PMHS01 (no pelvis injury). Future studies should include more comprehensive analyses of such anatomical variation to understand why PMHS sustained fractures at different locations. The main goal of the inertial loading estimation presented here was to explore if the inertial loading from the lower limb was large enough to possibly generate acetabulum fractures of the PMHS in HSRFFIs. It should be noted that loading rates and loading mechanisms are different (applied force to the knee using an impactor vs. inertial force from the lower limb). In addition to this, while the friction force between the PMHS and the seat pan would not be

negligible, it has been found that PMHS often unload the seat pan in moderate-speed rear impact scenarios [15] (Fig. B1) as the PMHS move rearward and away from the seat pan angle, e.g., tilt up. Therefore, the friction force from the seat pan in rear impacts becomes much smaller than that from frontal impacts. Even though whole-body masses (77.1kg for PMHS5, 92.1kg for PMHS11) and friction coefficients of 0.58 (highest dynamic friction coefficient reported in [16]) are considered in the estimations as a worst-case scenario, friction forces range from 0.44 to 0.52kN (0.58x77.1x9.81 = 439N and 0.58x92.1x9.81 = 524N), which are much smaller than the estimated inertial loading from the thigh (5.8kN – 6.0kN).

Superior and inferior pubic rami fractures with SI joint damage are usually caused by high-energy trauma associated with motor vehicle crashes [17]. In the simulated frontal impact PMHS experiment [13], seven of nineteen PMHS also sustained pubic rami fractures with (N=6) and without (N=1) acetabular fractures. The force measured for PMHS that sustained pubic ramus fractures in [13] ranged from 3.3kN to 6.7kN, similar to the inertial loading that the PMHS experienced in the current study. A pelvic outward deformation (pelvic open book) of the PMHS that was demonstrated by iliac wing off-axis rotations about global X- and Z-axes was discovered as a potential injury mechanism in a previous study [6]. However, the angular velocities of each iliac wing with respect to a local pelvic coordinate system have not yet been discussed. Figure 7 shows a potential injury mechanism of pelvic open-book deformations caused by torques induced by eccentric loads between seat back reaction at the posterior ilium and lower limb inertial load through the acetabulum. Unlike findings from the previous study [6], i.e., large off-axis rotations about the global X- and Z-axes, angular velocities only about the local z-axis exhibited a meaningful trend between injurious PMHS (pubic ramus fractures) and non-injurious PMHS (no pubic ramus fractures). The angular velocities about the local z-axis measured from injurious and non-injurious PMHS are shown in Fig. 8. It should be noted that peak angular velocities about the z-axis occurred at 41.90ms for PMHS09, 43.35ms for PMHS10, and 42.65ms for PMHS12 while the PMHS were pocketing into the seat back and began to ramp up along the seat back. Off-axis rotations about global X- and Z-axes were proposed as a potential injury criterion in the previous study [6]. Timing of the peak off-axis rotations was around 60ms based on the results from the previous study [6], which is later than the peak z-angular velocity timing measured in the current study. Peak timing of the femur linear accelerations, i.e., peak inertial loads from the lower limb, were also close to the z-angular velocity timing. Therefore, angular velocity about the local z-axis could be a potential injury parameter that can indicate the pelvic open-book injury mechanism.

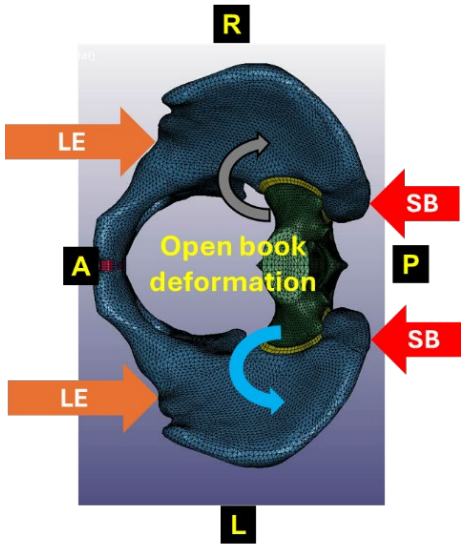

Fig. 7. A diagram for Pelvic open-book deformation due to torques caused by eccentric loadings from seat back reaction loads (red arrows labelled as SB) and lower limb inertial loads (orange arrows labelled as LE). Black and blue arrows represent open-book deformation on each iliac wing. A: anterior, P: posterior, L: left, R: right.

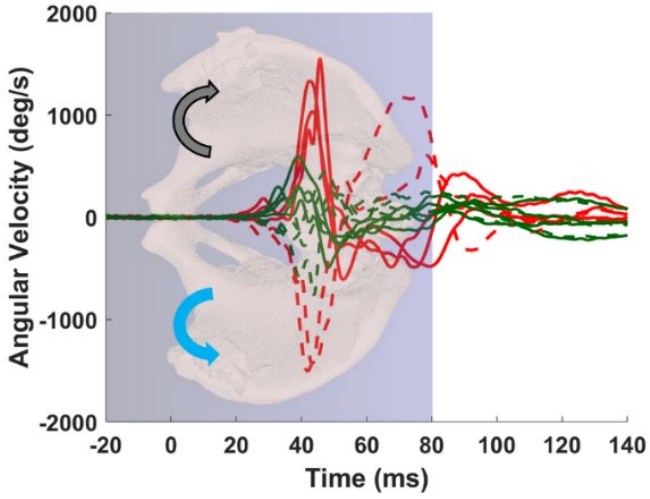

Fig. 8. Angular velocities about the local z-axis. Solid and dash lines are measured and transformed from the right and left iliac wings, respectively. The red represents angular velocities from injurious PMHS (PMHS09, PMHS10, and PMHS12), and the green indicates angular velocities from non-injurious PMHS. Positive and negative angular velocities represent gray and light blue circled arrows.

Posterior pelvic injuries, e.g., ilium fractures and SI joint damage, can be explained by direct pelvic interaction with the seat back. Figure 9 shows exemplary initial orientations of the pelves (PMHS21 and PMHS22) reconstructed using CT and X-ray images. In the 25deg reclined angle condition (Fig. 9a), the posterior pelvic region (more specifically posterior ilium and sacrum) directly interacted with the front surface of the seat back at the initial position (interaction with seat back foam) and would experience stress concentration while the PMHS was pocketing into the seat back. As the seat back foam bottoms out, seat back structures possibly influenced load distributions on the posterior pelvis and the injury outcomes. The information regarding the seat back foam thickness and structure is provided in Fig. 2. It should be noted that all three PMHS tested in ABTS25 did not sustain any pelvis fractures, while all four PMHS tested in FDR25 sustained injuries on the posterior pelvis, likely due to the difference in the seat back foam thicknesses and structures (Fig. 2). Differences in the seat back structures resulted in noticeable differences in angular velocity about the y-axis between PMHS tested in ABTS25 (especially PMHS02 and PMHS06) and those in FDR25 as shown in Fig. A5. PMHS02 and PMHS06 exhibited positive (rearward) angular velocities about the y-axis as a primary response, while all PMHS tested in FDR25 that sustained posterior pelvic injuries had negative (forward) angular velocities. Additionally, peak linear x-accelerations measured from PMHS tested in FDR25 (156.7 - 202.0g) were greater than those from ABTS25 (91.4 - 166.5g), which could also be affected by the differences in the seat back thicknesses and structures. In the 45deg reclined angle condition, the posterior sacral region first interacted with the seat back (Fig. 9b). It should be noted that none of the PMHS sustained sacrum fractures, regardless of the recline angles or seat types. All three PMHS tested in FDR45 sustained posterior pelvic injuries, while only one PMHS (PMHS04) tested in ABTS45 sustained these injuries. In the 45deg conditions, no noticeable differences in angular velocity about the y-axis between ABTS45 and FDR45 were observed (Fig. A5). However, peak linear x-accelerations in FDR45 were greater (ranging from 131.2 to 212.5g) than those from ABTS (ranging from 103.8 to 135.7g, excluding PMHS05 due to the left acetabular fracture). The seat back foam thickness and structure influenced the linear acceleration and possibly posterior pelvic injuries in the 45deg recline conditions.

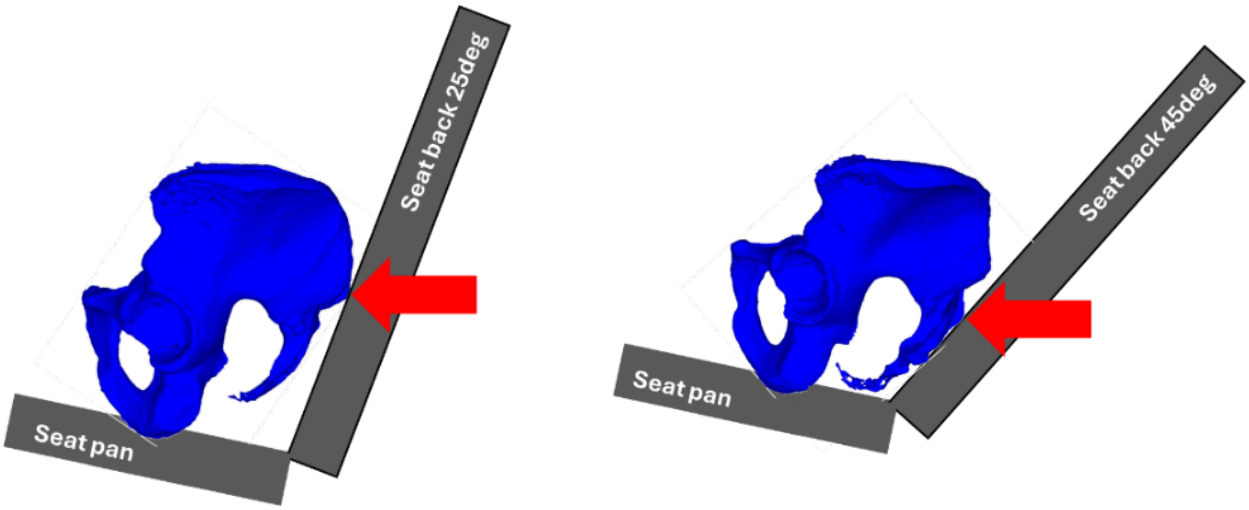

(a) PMHS21 (FDR25) (b) PMHS22 (FDR45)

Fig. 9. Initial pelvic orientation with respect to reclined seat back. Arrows represent initial contact regions.

Limitations

Only two seats were utilised in the current study. The foam properties, thickness, and density, as well as different seat back structures, could affect pelvic injury outcomes. Once ATDs and HBMs are improved and validated against data from the current study, parametric studies could be performed by changing seat foams and structure designs.

In order to ensure repeatability and durability, the seats were reinforced, which could influence pelvic injuries in the current study. Reinforced seat back conditions used in this study could be deemed as an extreme case with a stiff seat back. However, the information from this study should provide valuable insights into future seat back

designs. If rotational or yielding seat backs are used, pelvic linear acceleration may decrease, and the risk of pelvic injuries may be reduced. More PMHS and ATD experiments and HBM simulations are required to confirm the benefits of deformable seat backs for pelvic injury mitigation.

Only two OEM seats were used in this study. Foam and internal structure of seat backs could influence injury outcomes. The effect of the seat back foam and internal structure on injury outcomes should be investigated and possibly optimized to mitigate injuries in rear-facing scenarios.

Strain gages were not installed on the PMHS pelvis tested in this study, so the timing of the fractures could not be identified. Although some acceleration signals indicated sudden changes and possible fracture timing, using strain gages will be more beneficial and produce accurate fracture timing and strain modes (tensile vs. compressive strains). Strain gages have been attached to the right and left superior pubic rami for all recent PMHS tests to learn more about fracture timing and strain mode, which will be discussed in a future study.

Types of pelvic injuries resulting from severe rear-facing or rear-impacts have not been discussed in the literature. There are limited high-speed rear impact cases in which an occupant sustained pelvic fractures in the Crash Injury Research Engineering Network (CIREN) database and Crash Investigation Sampling System (CISS). However, CIREN and CISS have been collecting more high-speed rear-impact cases in which occupants sustained pelvis fractures. These CIREN cases will be discussed further in a future study. PMHS experimental data and real-world injury cases from CIREN should aid in understanding injury mechanisms of the pelvis in high-speed rear-facing impacts.

V. CONCLUSION

In this study, male PMHS sustained posterior pelvic fractures (PSIS and SI joint damage) and pubic ramus fractures. The 6DX motion blocks installed at each iliac wing provided important information regarding pelvis deformation in HSRFFI scenarios and helped to understand the pubic ramus fracture mechanism. Pelvis open-book deformation was demonstrated by large z-angular velocities measured at each iliac wing while the PMHS pocketed into the seat backs. Inertial loading of the lower limb affected acetabular fractures. The seat back frame design affected the direction of the pelvic angular velocity about the y-axis and linear x-acceleration, possibly influencing injury outcomes. Since pelvis responses and resulting injuries in HSRFFIs are lacking in the literature, the novel results from this study could be used to improve biofidelity of ATDs and finite element HBMs.

VI. ACKNOWLEDGEMENTS

We would like to thank anatomical donors sincerely. Without their generous donations, this study could not have been done. We would also like to thank students, staff, and faculty from the Injury Biomechanics Research Center at The Ohio State University for their valuable support of the PMHS experiments.

This paper is published in the interest of advancing motor vehicle safety research. The opinions, findings, and conclusions expressed in this publication are those of the authors and not necessarily those of the U.S. Department of Transportation (DOT) or National Highway Traffic Safety Administration (NHTSA). The United States Government assumes no liability or responsibility for its contents or use thereof. If trade or manufacturers' names or products are mentioned, it is only because they are considered essential to the object of the publication and should not be construed as an endorsement. The United States Government does not endorse products or manufacturers. While the report may provide results from research or tests using specifically identified motor vehicle models, it is not intended to make conclusions about the safety performance or safety compliance of those motor vehicles, and no such conclusions should be drawn.

VII. REFERENCES

[1] SAE. Taxonomy and Definitions for Terms Related to Driving Automation Systems for On-Road Motor Vehicles. *Society of Automotive Engineers*, 2021, Paper No. J3016_202104.

[2] Jorlöv, S., Bohman, K., Larsson, A. Seating positions and activities in highly automated cars–a qualitative study of future automated driving scenarios. *Proceedings of International Conference on the Biomechanics of Impact (IRCOBI)*, 2017, IRC-17-11, Antwerp, Belgium.

[3] Koppel, S., Jiménez Octavio, J., Bohman, K., Logan, D., et al. Seating configuration and position preferences in fully automated vehicles. *Traffic injury prevention*, 2019, **20**(sup2): S103-S109.

[4] Östling, M., Larsson, A. Occupant activities and sitting positions in automated vehicles in China and Sweden. *Proceedings of 26th International Technical Conference on the Enhanced Safety of Vehicles (ESV)*, 2019, pp. 10-13.
[5] Kang Y., Stammen J., Ramachandra R., Agnew A.M., Hagedorn A., Thomas C., Kwon H.J., Moorhouse K., Bolte J.H. Biomechanical responses and injury assessment of post mortem human subjects in various rear-facing seating configurations. *Stapp Car Crash Journal*, 2020, **64**: 155–212.
[6] Kang Y., Stammen J., Bendig A., Agnew A.M., Hagedorn A., Thomas C., Ramachandra R., Kwon H.J., Moorhouse K., Bolte J.H. Effects of seat back recline and belt restraint type on PMHS responses and injuries in rear-facing frontal impacts. *SAE International Journal of Transportation Safety*, 2022, **10**(2):235–289.
[7] Kang Y., Stammen J., Agnew A., Baker G., Pradhan V., Bendig A., Hagedorn A., Moorhouse K., Bolte J. Thoracic responses and injuries to male postmortem human subjects (PMHS) in rear facing seat configurations in high-speed frontal impacts. *Traffic Injury Prevention*, 2023, **24**(sup1): S47-S54.
[8] Davidsson J., Deutscher C., Hell W., Linder A., Lövsund P., Svensson M.Y. Human volunteer kinematics in rear-end sled collisions. *Proceedings of International Conference on the Biomechanics of Impact (IRCOBI)*, 1998, pp. 289-301, Gothenburg, Sweden.
[9] Philippens M., Wismans J., Cappon H., Yoganandan N., Pintar F. Whole body kinematics using post mortem human subjects in experimental rear impact. *Proceedings of International Conference on the Biomechanics of Impact (IRCOBI)*, 2000, pp. 363-378, Montpellier, France.
[10] White N.A., Begeman P.C., Hardy W.N., Yang K.H., Ono K., Sato F., Kamiji K., Yasuki T., Bey M.J. Investigation of upper body and cervical spine kinematics of post mortem human subjects (PMHS) during low-speed, rear-end impacts. *SAE Technical Paper*, 2009, Paper No. 2009-01-0387.
[11] Mertz H.J., Jarrett K., Moss S., Salloum M., Zhao Y. The Hybrid III 10-year-old dummy. *SAE Technical Paper*, 2001, Paper No. 2001-22-0014.
[12] SAE. Instrumentation for Impact Test - Part 1 Electronic instrumentation. *Society of Automotive Engineers,* 2014, Paper No. J211/1_202208.
[13] Rupp J.D., Reed M.P., Van Ee C.A., Kuppa S., Wang S.C., Goulet J.A., Schneider L.W. The tolerance of the human hip to dynamic knee loading. *Stapp Car Crash Journal*, 2002, **46**: 211-228.
[14] Fellin R., O'Donovan M., McKenzie K., Bensel C., Albery C. Comparison of body segment masses in male and female postmortem human specimens. *Proceedings of Sixth International Congress on Soldiers' Physical Performance (ICSPP)*, 2023, London, UK.
[15] Kang, Y. S., Moorhouse, K., Donnelly, B., Herriott, R., Mallory, A., Bolte, J. Biomechanical responses of PMHS in moderate-speed impacts and development of response targets for evaluating the internal and external biofidelity of ATDs. *Stapp Car Crash Journal*, 2012, **56**: 105–170.
[16] Scott J, Bush TR. Determining frictional properties of pants and cushion cover materials using human soft tissue and a rigid sled and how they affect seated shear forces. *Journal of Biomechanics*. 2023, **1(**147).
[17] Tile M. Acute pelvic fractures: I. Causation and classification. *Journal of the American Academy of Orthopaedic Surgeons*, 1996, **4**(3):143-151.

VIII. APPENDIX

Appendix A

TABLE AI
RELEVANT ANTHROPOMETRY MEASUREMENTS

Test condition	PMHS#	Hip Breadth (cm)	Hip Circumference (cm)	Waist Breadth (cm)	Waist Depth (cm)	Waist Circumference (cm)
ABTS45	PMHS01*	32.5	90.0	28.6	18.9	84.6
	PMHS04*	33.4	100.4	32.6	25.2	112.0
	PMHS05*	32.1	98.8	30.7	18.2	93.2
FDR45	PMHS09**	34.6	100.6	34.4	18.1	99.9
	PMHS13**	32.7	97.4	26.2	18.4	94.0
	PMHS22***	32.2	94.5	31.2	18.0	97.2
ABTS25	PMHS02*	32.6	94.3	29.7	18.3	89.5
	PMHS03*	35.7	105.9	32.9	22.8	99.6
	PMHS06*	33.2	95.0	31.3	18.4	94.2
FDR25	PMHS10***	33.0	101.5	33.2	21.0	106.4
	PMHS11**	36.9	105.0	34.5	21.7	99.8
	PMHS12**	32.8	90.3	29.1	19.0	87.5
	PMHS21***	33.1	90.9	28.2	20.3	84.8
Mean (SD)	N/A	33.4 (1.4)	97.3 (5.3)	31.0 (2.5)	19.9 (2.2)	95.6 (8.1)

* [5]; ** [6]; *** [7]

TABLE AII
PEAK LINEAR ACCELERATION TIMING

Test condition	PMHS#	x-direction		y-direction		z-direction	
		Left	Right	Left	Right	Left	Right
ABTS45	PMHS01	43.05	39.25	45.20	44.55	46.70	44.70
	PMHS04	42.50	44.35	42.05	44.55	48.75	44.65
	PMHS05	44.65	38.50	43.10	43.85	44.00	49.35
FDR45	PMHS09	40.15	40.15	39.50	41.30	38.95	46.90
	PMHS13	42.40	45.80	49.05	45.65	42.50	42.00
	PMHS22	46.95	48.85	46.80	48.60	47.20	48.60
ABTS25	PMHS02	39.20	38.60	42.15	41.65	39.60	38.70
	PMHS03	39.15	39.00	44.00	37.50	40.60	48.75
	PMHS06	38.00	37.65	39.30	41.85	44.25	32.30
FDR25	PMHS10	40.95	44.55	41.15	44.40	41.55	43.95
	PMHS11	40.50	39.20	44.55	46.15	45.30	47.15
	PMHS12	42.35	41.45	42.45	41.65	41.90	40.40
	PMHS21	38.10	40.50	39.00	40.80	39.75	45.00

TABLE AIII
PEAK ANGULAR VELOCITY TIMING

Test condition	PMHS#	x-direction		y-direction		z-direction	
		Left	Right	Left	Right	Left	Right
ABTS45	PMHS01	53.00	44.10	63.40	66.10	43.85	48.20
	PMHS04	65.40	63.65	71.75	71.40	38.35	40.00
	PMHS05	45.50	47.75	67.80	66.50	43.95	45.20
FDR45	PMHS09	48.65	86.55	41.35	43.05	41.90	43.45
	PMHS13	43.20	48.65	60.00	59.10	43.05	43.10
	PMHS22	47.30	54.10	69.60	69.80	53.85	47.60
ABTS25	PMHS02	42.65	32.70	42.25	42.25	40.80	32.85
	PMHS03	70.40	68.35	41.35	43.00	47.65	38.95
	PMHS06	76.00	81.65	42.95	43.45	49.05	38.90
FDR25	PMHS10	80.70	46.80	41.00	41.50	43.35	45.70
	PMHS11	48.30	46.35	43.45	43.15	47.80	41.15
	PMHS12	43.35	40.35	42.95	42.45	43.25	42.65
	PMHS21	51.45	41.70	40.95	41.05	40.40	40.60

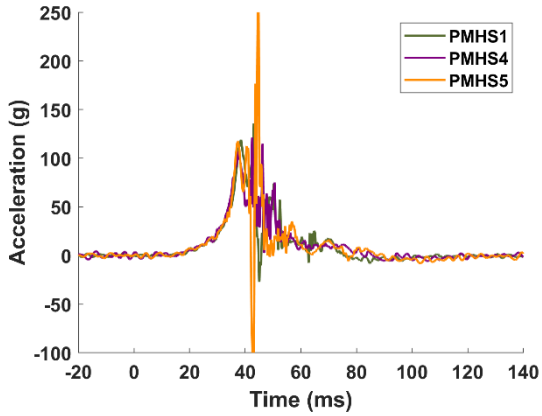

(a) ABTS45 Left

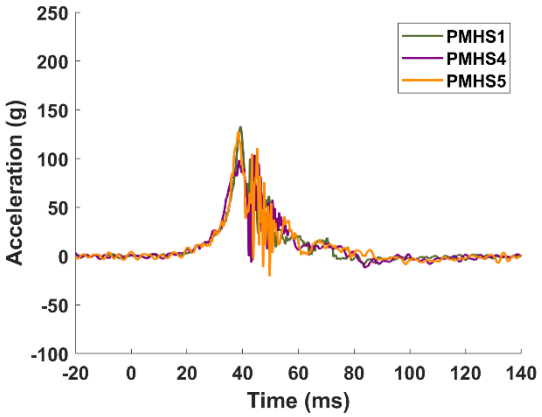

(b) ABTS45 Right

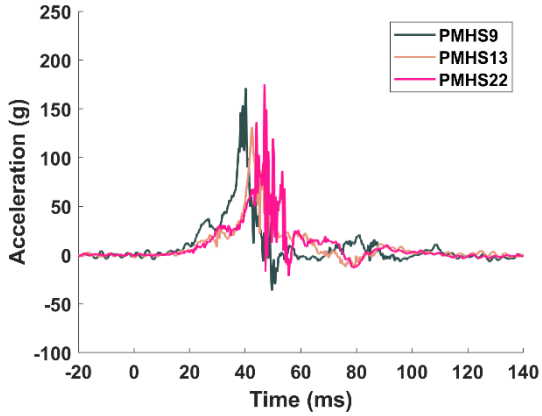

(c) FDR45 Left

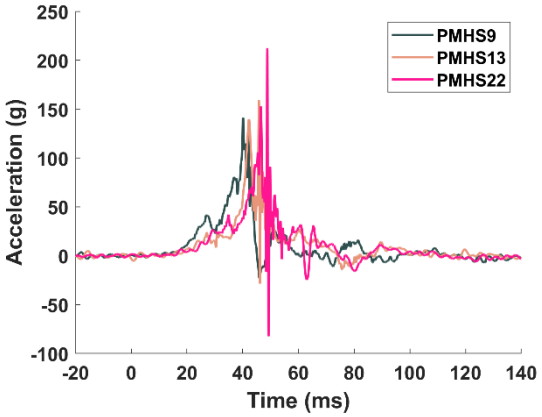

(d) FDR45 Right

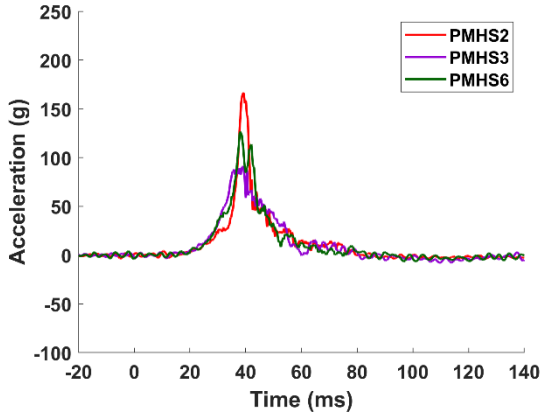

(e) ABTS25 Left

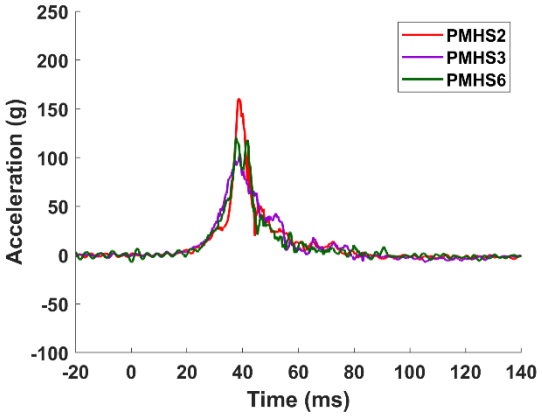

(f) ABTS25 Right

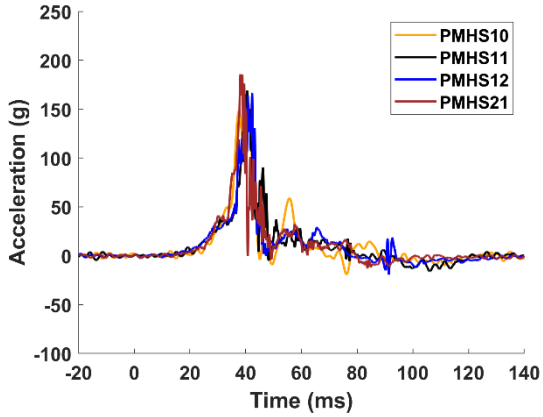

(g) FDR25 Left

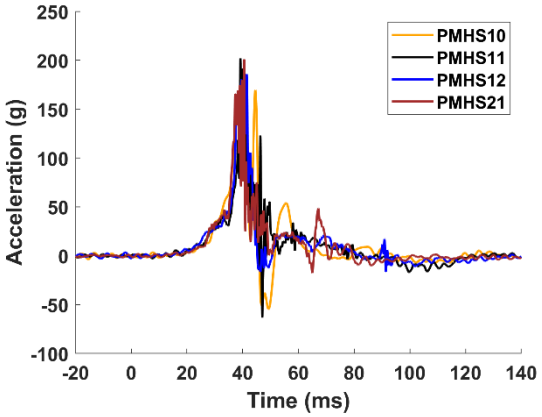

(h) FDR25 Right

Fig. A1. Acceleration in x-direction.

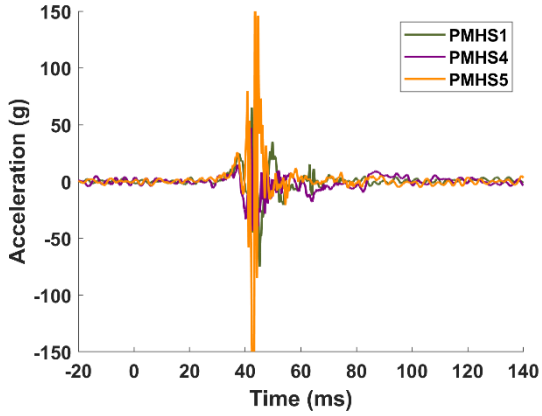

(a) ABTS45 Left

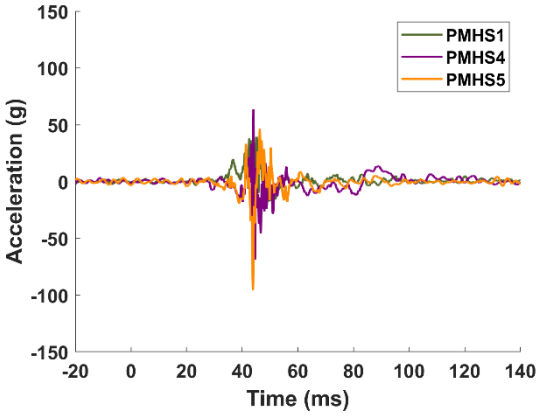

(b) ABTS45 Right

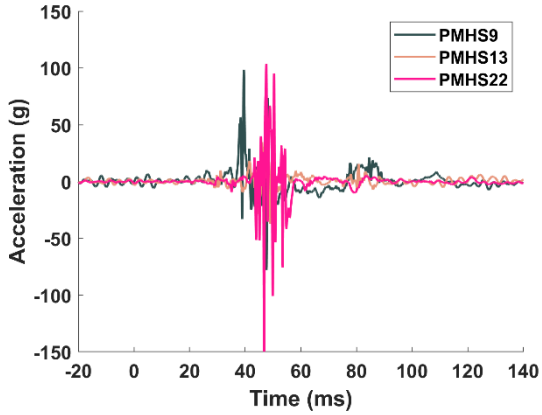

(c) FDR45 Left

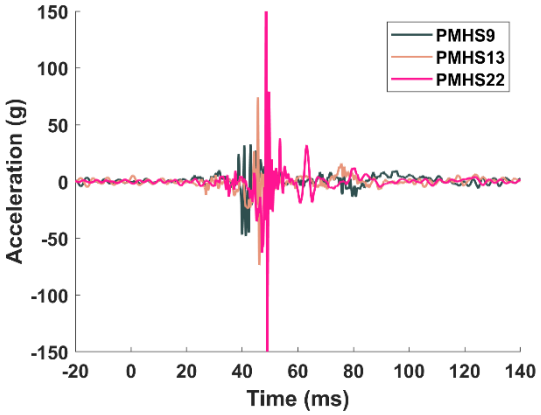

(d) FDR45 Right

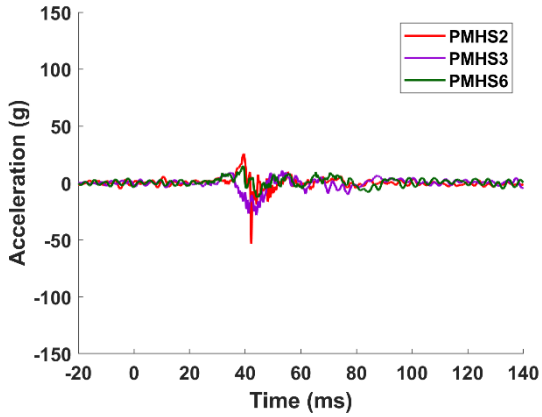

(e) ABTS25 Left

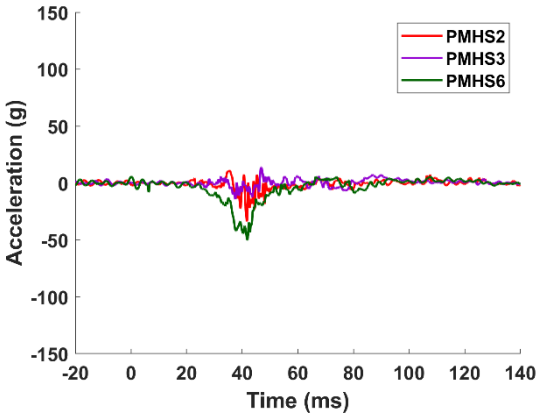

(f) ABTS25 Right

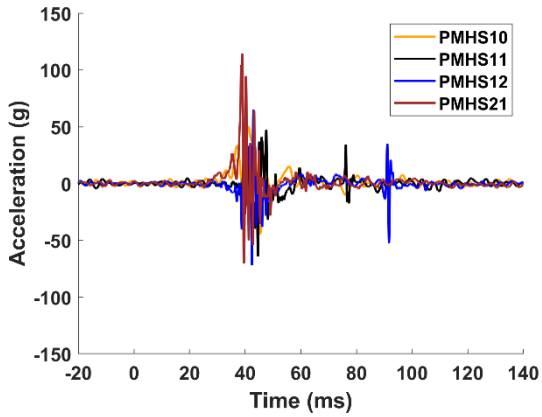

(g) FDR25 Left

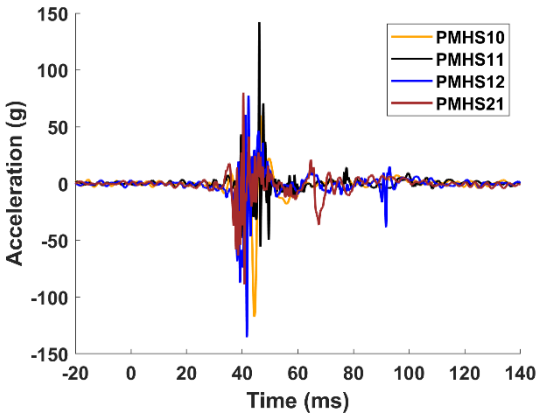

(h) FDR25 Right

Fig. A2. Acceleration in y-direction.

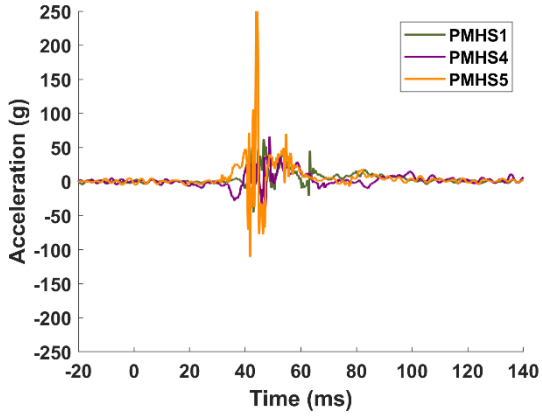

(a) ABTS45 Left

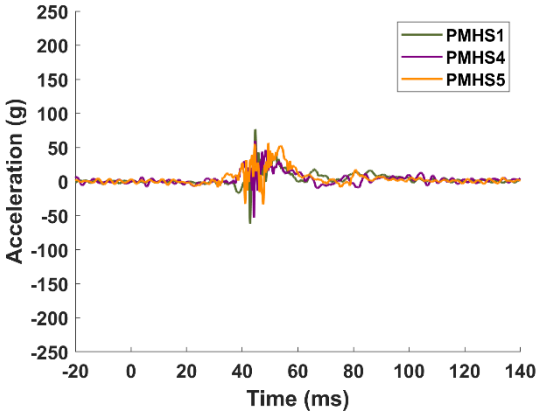

(b) ABTS45 Right

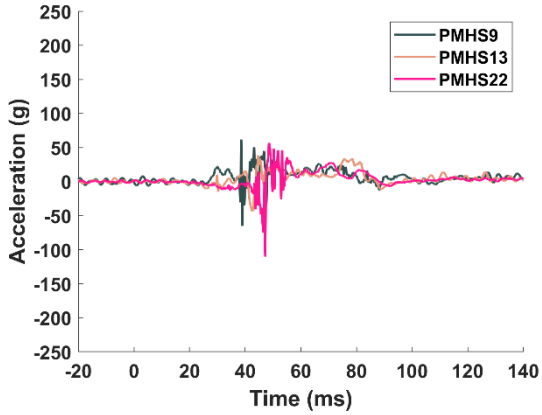

(c) FDR45 Left

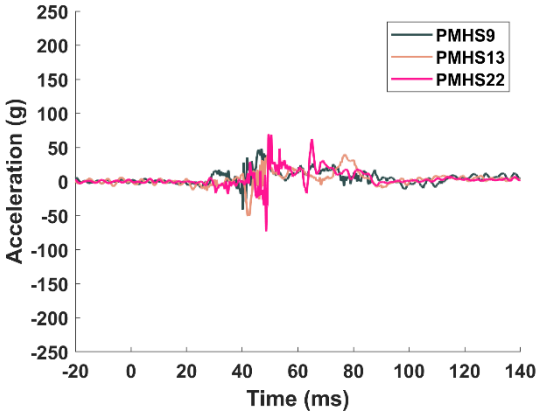

(d) FDR45 Right

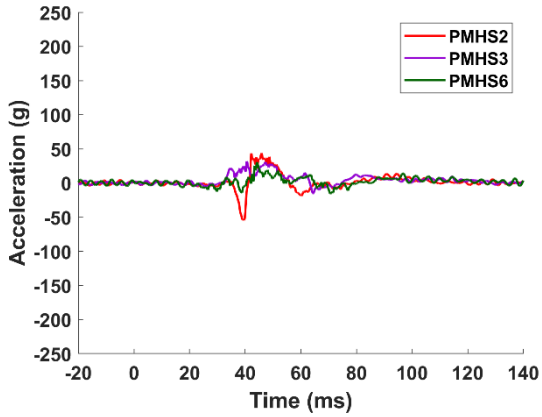

(e) ABTS25 Left

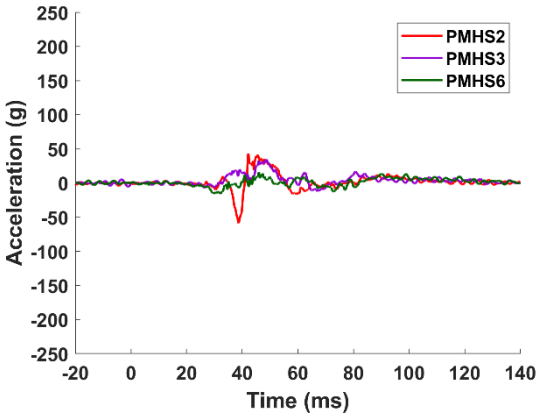

(f) ABTS25 Right

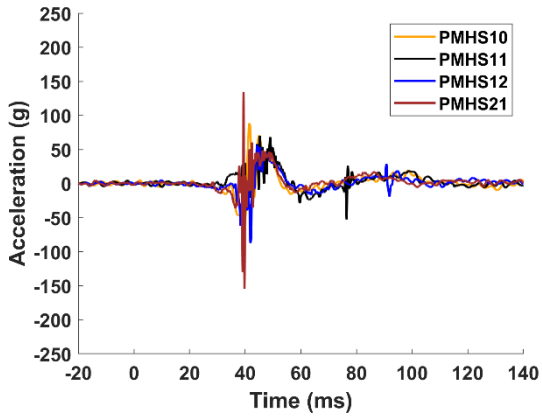

(g) FDR25 Left

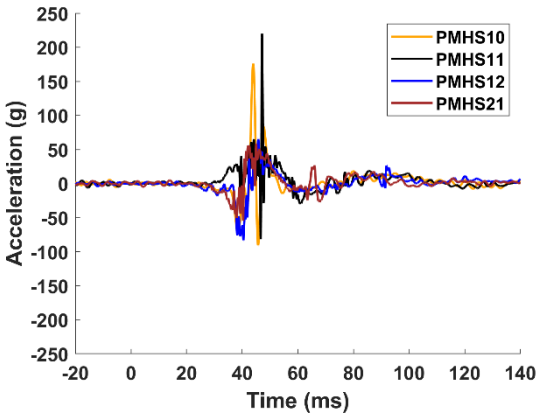

(h) FDR25 Right

Fig. A3. Acceleration in z-direction.

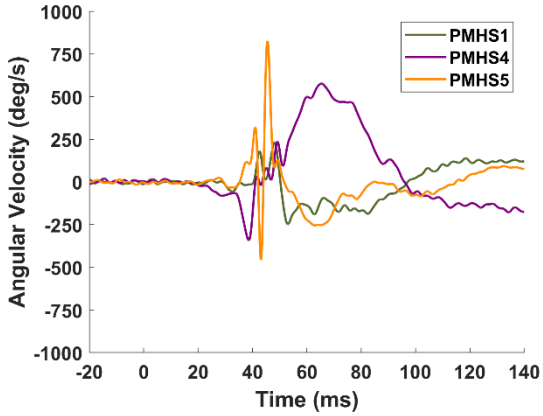

(a) ABTS45 Left

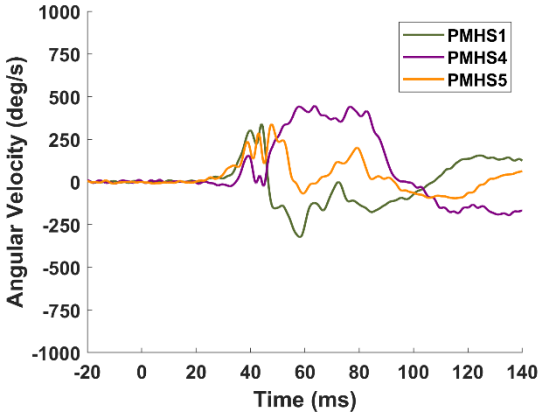

(b) ABTS45 Right

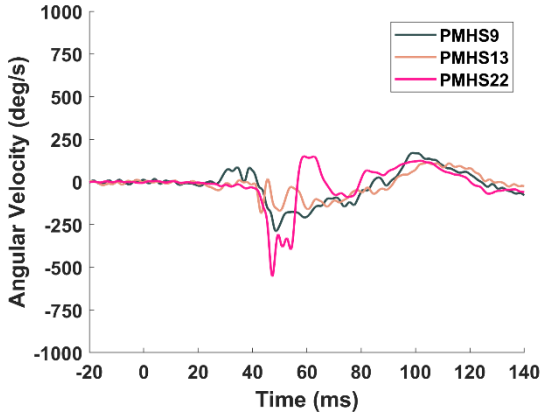

(c) FDR45 Left

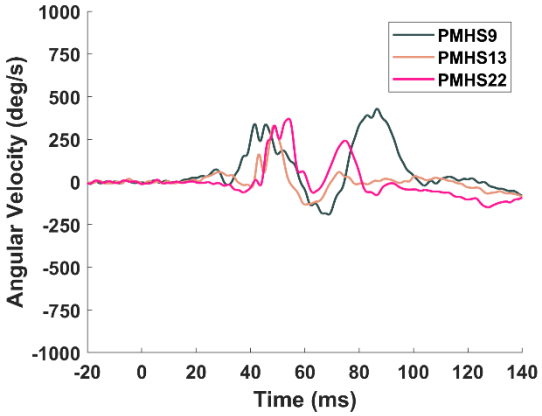

(d) FDR45 Right

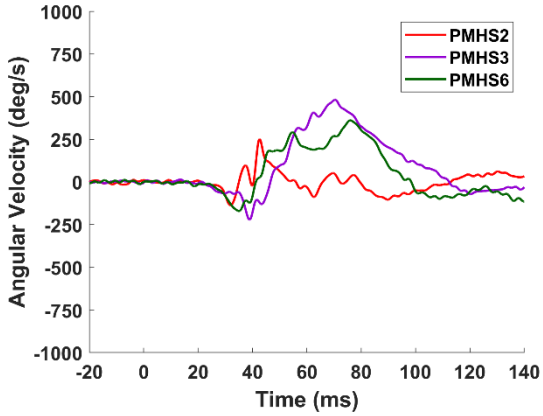

(e) ABTS25 Left

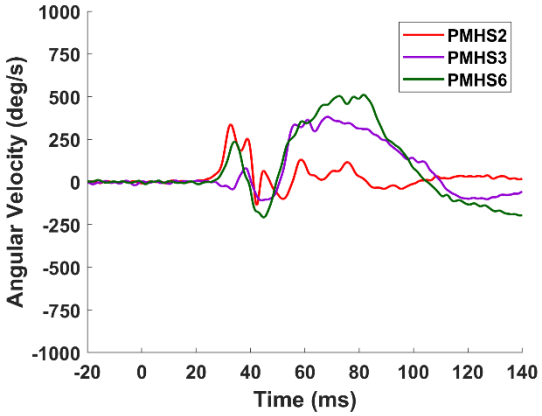

(f) ABTS25 Right

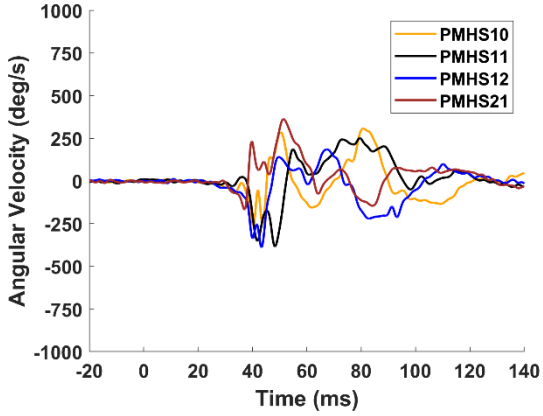

(g) FDR25 Left

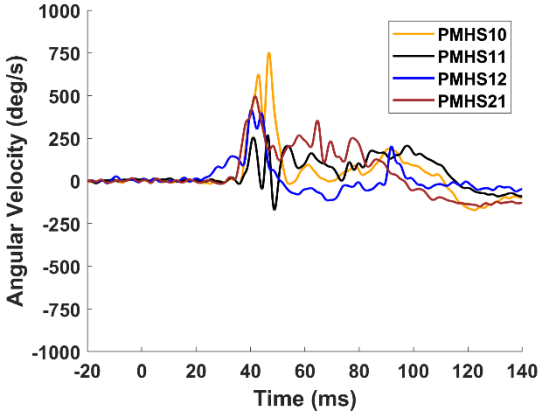

(h) FDR25 Right

Fig. A4. Angular velocity about x-axis.

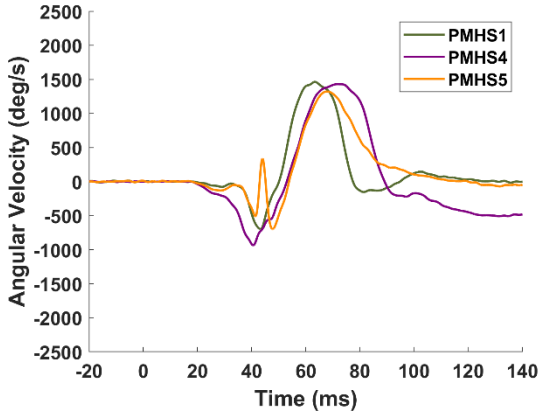

(a) ABTS45 Left

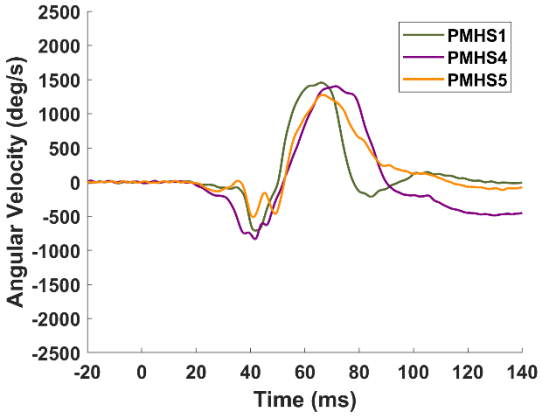

(b) ABTS45 Right

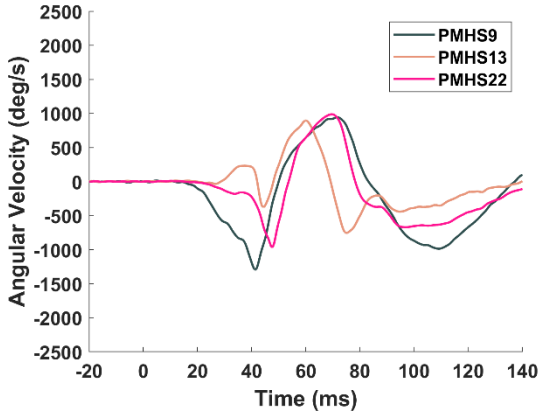

(c) FDR45 Left

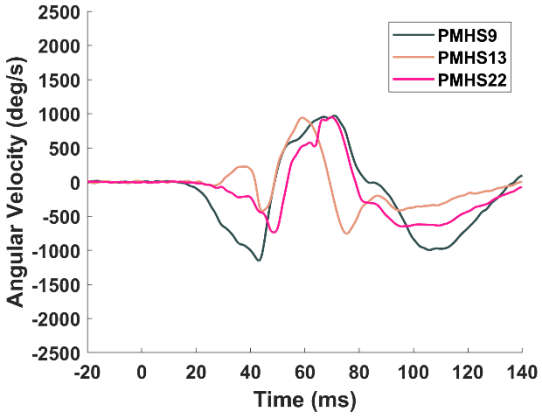

(d) FDR45 Right

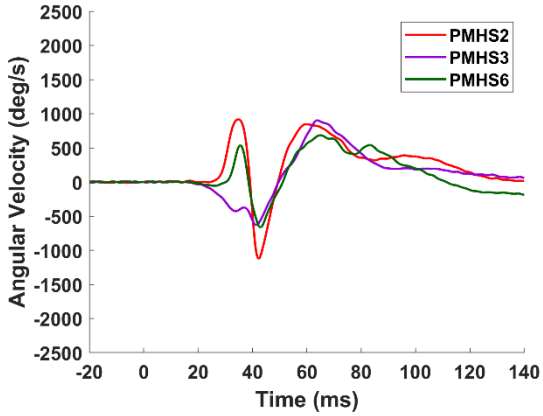

(e) ABTS25 Left

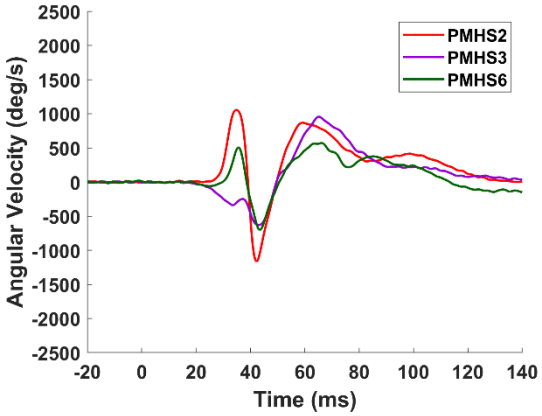

(f) ABTS25 Right

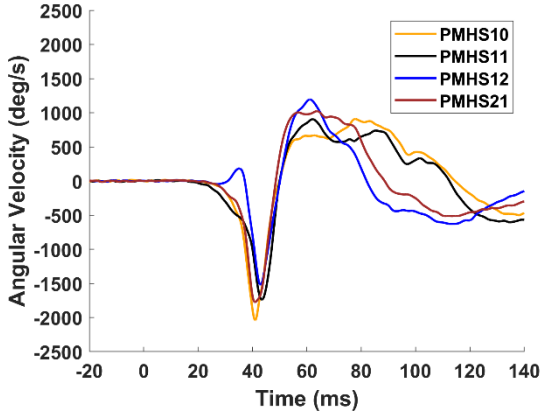

(g) FDR25 Left

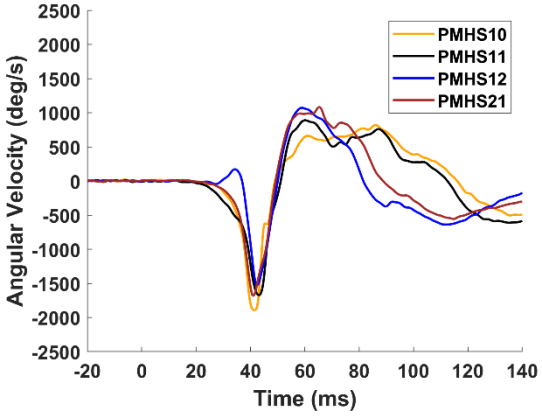

(h) FDR25 Right

Fig. A5. Angular velocity about y-axis.

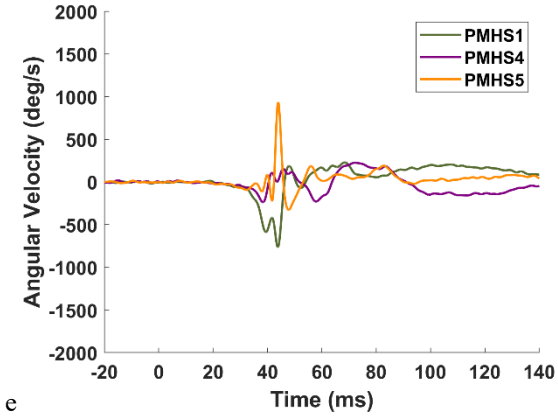

e

(a) ABTS45 Left

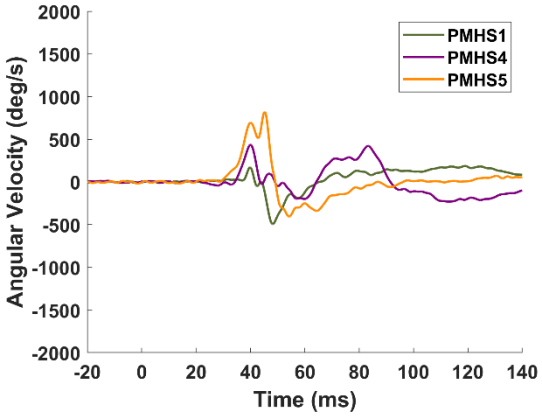

(b) ABTS45 Right

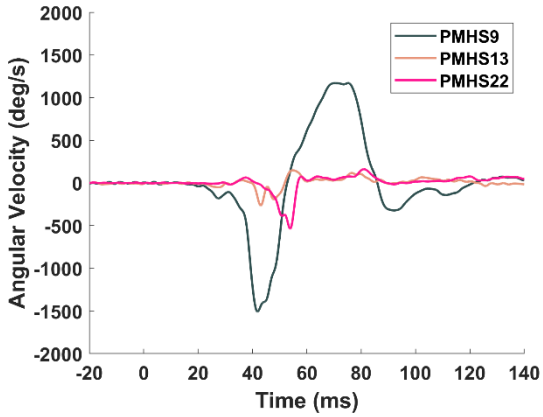

(c) FDR45 Left

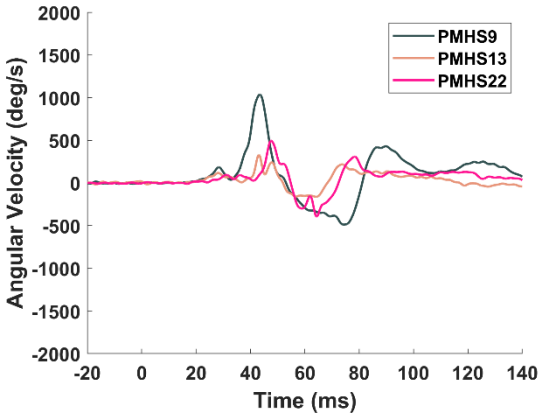

(d) FDR45 Right

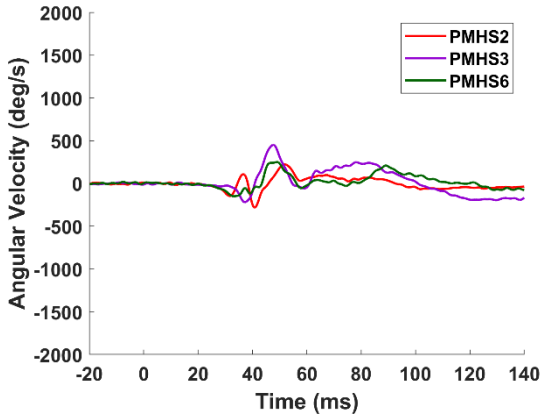

(e) ABTS25 Left

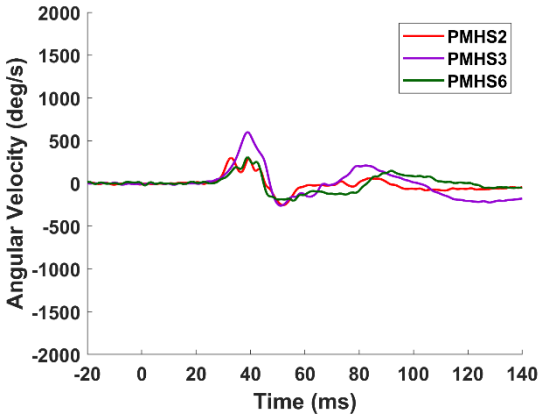

(f) ABTS25 Right

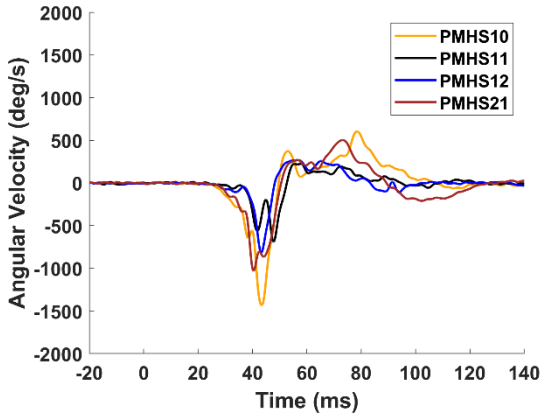

(g) FDR25 Left

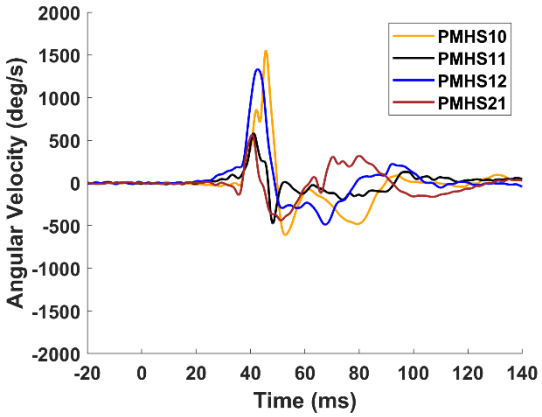

(h) FDR25 Right

Fig. A6. Angular velocity about z-axis.

Appendix B

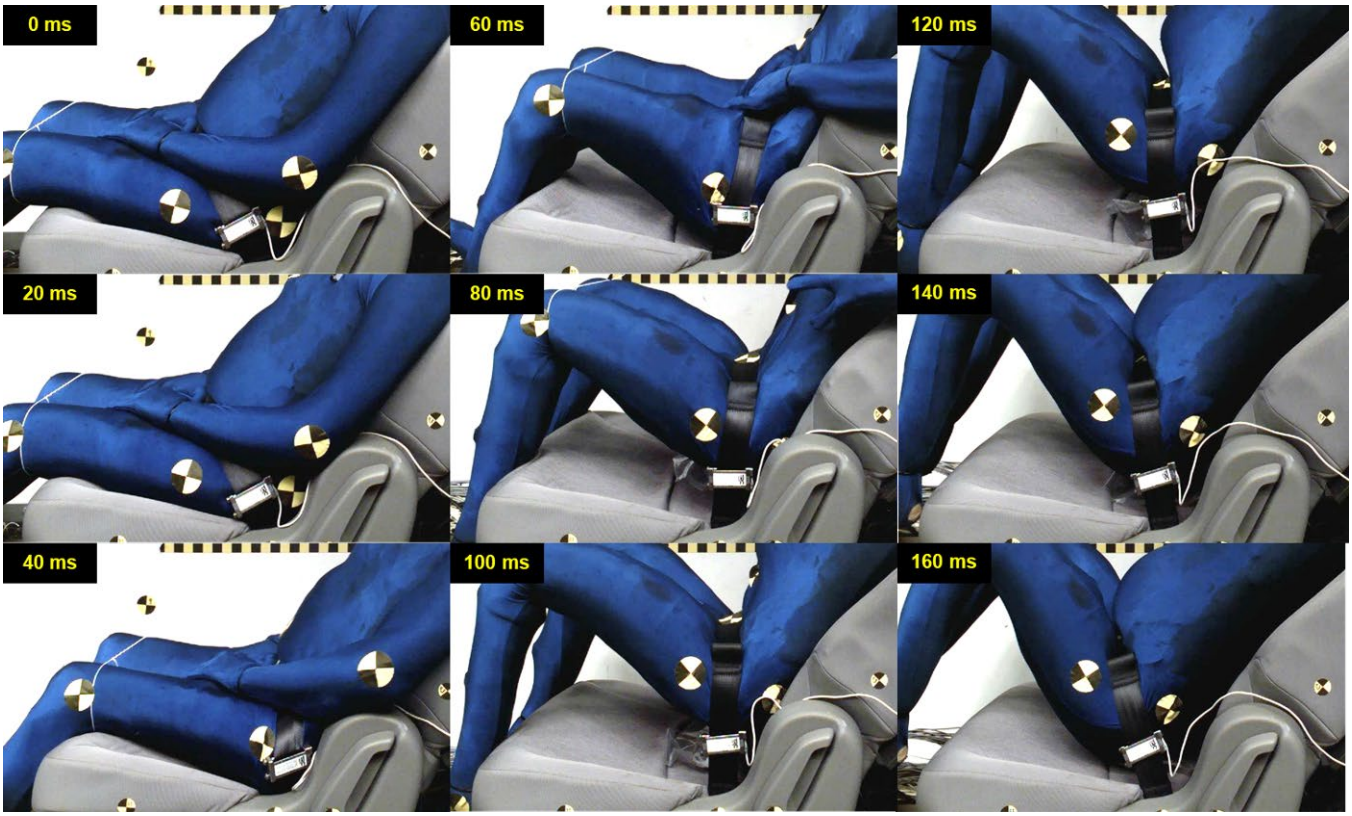

(a) ABTS45 (PMHS5)

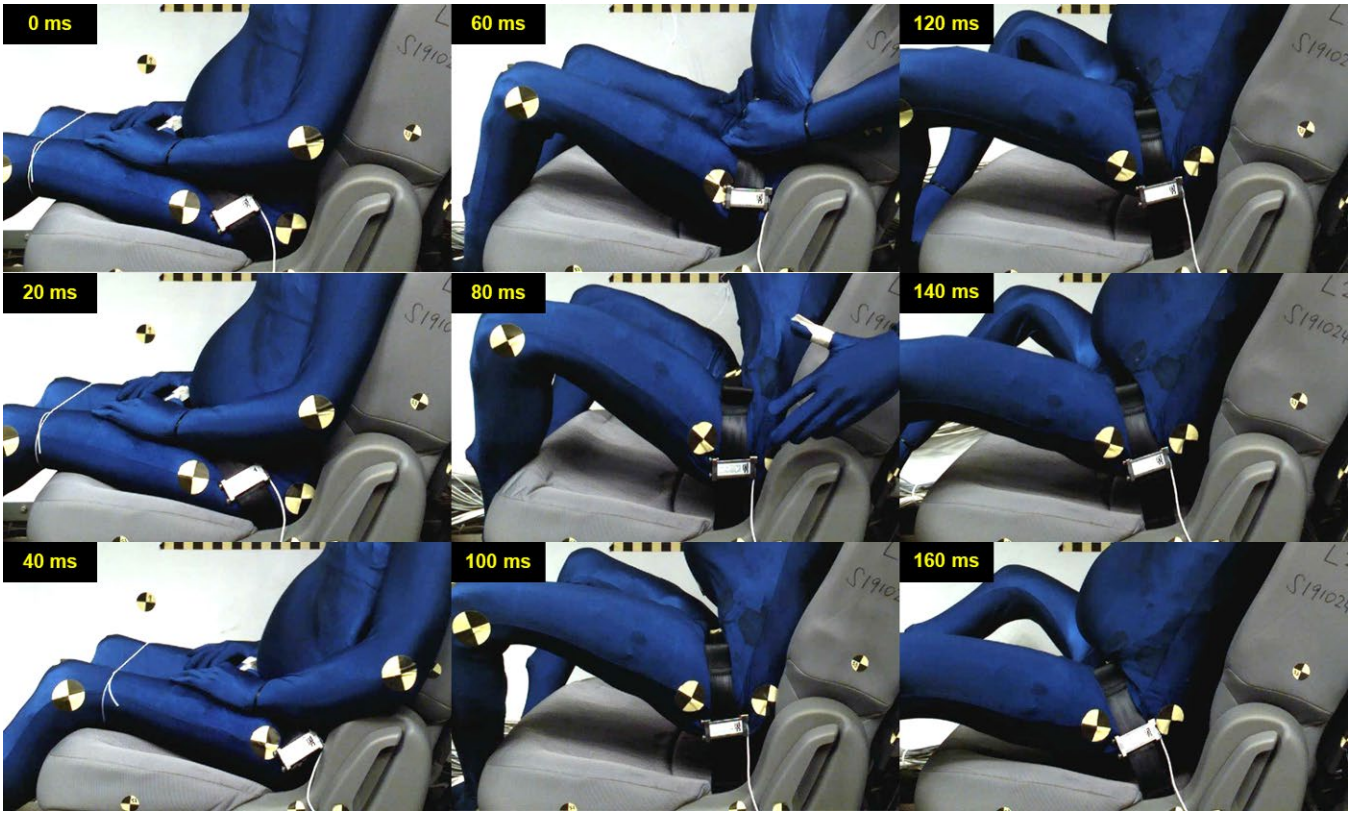

(b) ABTS25 (PMHS6)

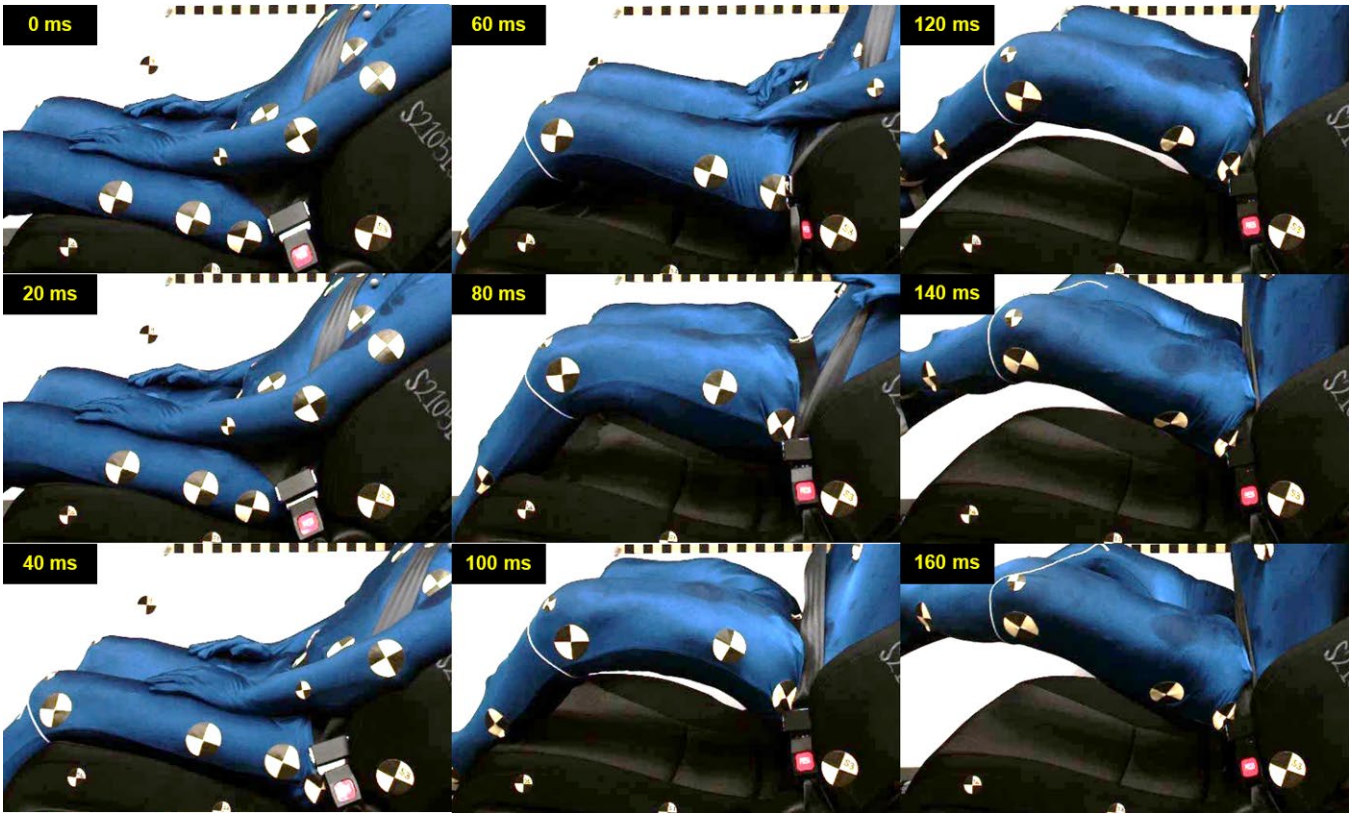

(c) FDR45 (PMHS22)

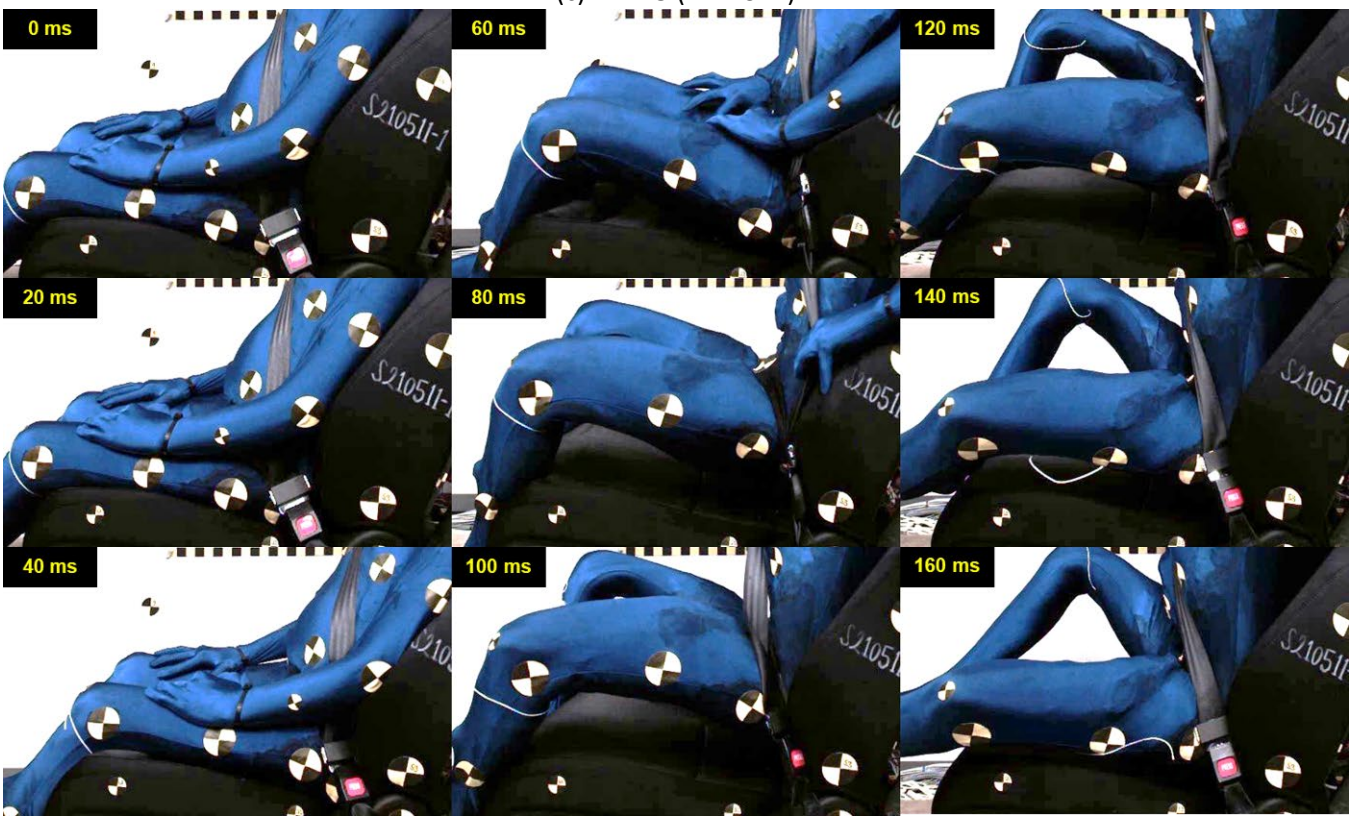

(d) FRD25 (PMHS21)

Fig. B1. Sequential motions focused on the pelvis region.